Received: 5 March 2020 | Accepted: 18 May 2020

DOI: 10.1111/gcb.15276

PRIMARY RESEARCH ARTICLE

Global Change Biology WILEY

An optimality-based model explains seasonal variation in C3 plant photosynthetic capacity

Chongya Jiang[1] | Youngryel Ryu[1] | Han Wang[2] | Trevor F. Keenan[3,4]

[1]Department of Landscape Architecture and Rural Systems Engineering, Seoul National University, Seoul, Korea

[2]Department of Earth System Science, Tsinghua University, Beijing, China

[3]Climate and Ecosystem Sciences Division, Lawrence Berkeley National Laboratory, Berkeley, CA, USA

[4]Department of Environmental Science, Policy and Management, UC Berkeley, Berkeley, CA, USA

Correspondence
Chongya Jiang and Youngryel Ryu, Department of Landscape Architecture and Rural Systems Engineering, Seoul National University, Seoul, Korea.
Email: chongya.jiang@gmail.com (C.J.); ryuyr77@gmail.com (Y.R.)

Funding information
NASA Terrestrial Ecology Program IDS Award, Grant/Award Number: NNH17AE86I; Korea Ministry of Environment, Grant/Award Number: 2019002760002; National Research Foundation of Korea, Grant/Award Number: NRF-2016M1A5A1901789 and NRF-2019R1A2C2084626; Seoul National University

Abstract

The maximum rate of carboxylation (V_{cmax}) is an essential leaf trait determining the photosynthetic capacity of plants. Existing approaches for estimating V_{cmax} at large scale mainly rely on empirical relationships with proxies such as leaf nitrogen/chlorophyll content or hyperspectral reflectance, or on complicated inverse models from gross primary production or solar-induced fluorescence. A novel mechanistic approach based on the assumption that plants optimize resource investment coordinating with environment and growth has been shown to accurately predict C3 plant V_{cmax} based on mean growing season environmental conditions. However, the ability of optimality theory to explain seasonal variation in V_{cmax} has not been fully investigated. Here, we adapt an optimality-based model to simulate daily $V_{cmax,25C}$ (V_{cmax} at a standardized temperature of 25°C) by incorporating the effects of antecedent environment, which affects current plant functioning, and dynamic light absorption, which coordinates with plant functioning. We then use seasonal $V_{cmax,25C}$ field measurements from 10 sites across diverse ecosystems to evaluate model performance. Overall, the model explains about 83% of the seasonal variation in C3 plant $V_{cmax,25C}$ across the 10 sites, with a medium root mean square error of 12.3 μmol m^{-2} s^{-1}, which suggests that seasonal changes in $V_{cmax,25C}$ are consistent with optimal plant function. We show that failing to account for acclimation to antecedent environment or coordination with dynamic light absorption dramatically decreases estimation accuracy. Our results show that optimality-based approach can accurately reproduce seasonal variation in canopy photosynthetic potential, and suggest that incorporating such theory into next-generation trait-based terrestrial biosphere models would improve predictions of global photosynthesis.

KEYWORDS

canopy structure, memory effect, optimality hypothesis, photosynthetic capacity, terrestrial biosphere model, V_{cmax}

1 | INTRODUCTION

Great advances have been achieved in representing photosynthesis in terrestrial biosphere models (TBMs; Fisher, Huntzinger, Schwalm, & Sitch, 2014; Ryu, Berry, & Baldocchi, 2019), yet substantial uncertainties still exist in terms of total amount, spatial distribution, seasonal cycle, and interannual variation of carbon uptake by plants (Anav et al., 2015; Baldocchi, Ryu, & Keenan, 2016). One source of uncertainty in TBMs lies in the assumption of constant plant leaf traits for different plant functional types (PFTs; Wullschleger et al., 2014; Yang, Zhu, Peng, Wang, & Chen, 2015). This assumption accounts for first-order variation but overlooks spatial variation

within PFTs (Kattge et al., 2011; Wright et al., 2005) and temporal variation due to acclimation and adaptation (Evans & Poorter, 2001; Lavergne, Mouquet, Thuiller, & Ronce, 2010).

The maximum rate of carboxylation (V_{cmax}), a key leaf trait determining photosynthetic capacity of plants (von Caemmerer, Farquhar, & Berry, 2009; Farquhar, Caemmerer, & Berry, 1980), is widely treated as a prescribed PFT-dependent parameter in TBMs (Bonan et al., 2011; Harper et al., 2016). Yet plant CO_2 uptake quantified by PFT-based TBMs is theoretically inadequate to represent reasonable impacts and feedback between vegetation and the environment (Rogers et al., 2016; Scheiter, Langan, & Higgins, 2013). In this context, next-generation trait-based TBMs have emerged in recent years (Pavlick, Drewry, Bohn, Reu, & Kleidon, 2013; Van Bodegom, Douma, & Verheijen, 2014). It is highly desirable to develop sound methods of modeling, mapping, and monitoring V_{cmax} to improve TBMs in a spatiotemporally explicit manner.

Attempts to estimate V_{cmax} at large scale fall into three general categories. The first is statistical approaches. Efforts have been made to empirically link V_{cmax} field measurements with various proxies, including climate data (Ali et al., 2015; Verheijen et al., 2013), hyperspectral leaf/canopy reflectance (Dechant, Cuntz, Vohland, Schulz, & Doktor, 2017; Serbin et al., 2015), vegetation indices (Alton, 2017; Zhou et al., 2014), leaf chlorophyll content (LCC; Houborg, McCabe, Cescatti, Gao, et al., 2015; Luo, Croft, Chen, He, & Keenan, 2019), and leaf nitrogen content (LNC; Kattge, Knorr, Raddatz, & Wirth, 2009; Walker et al., 2014). Given the limited number and distribution of measured V_{cmax}-proxy pairs globally, the robustness of statistical models at large scales is unclear. In particular, many of them rely on PFT-dependent relationship, which implies an inability to explain the spatiotemporal variation in V_{cmax}.

The second category is inversion approaches. TBMs are calibrated or assimilated using tower-measured gross primary productivity (GPP; Dutta, Schimel, Sun, Van Der Tol, & Frankenberg, 2019; Zheng et al., 2017) or satellite-observed sun-induced chlorophyll fluorescence (SIF) data (He et al., 2019; Zhang, Guanter, et al., 2014; Zhang, Guanter, Joiner, Song, & Guan, 2018). Optimized V_{cmax} values yielding best model-data agreements are considered as retrievals. However, GPP observations are unavailable at large scale, and satellite-based GPP estimations are characterized by large uncertainty (Stocker, Zscheischler, et al., 2019; Xiao et al., 2019). By contrast, SIF observations are usually limited by temporal coverage, spatial resolution, signal-to-noise ratio, cloud and aerosol contamination, atmospheric and angular effects, or sensor degradation (Joiner, Yoshida, Guanter, & Middleton, 2016; Zhang, Joiner, Gentine, & Zhou, 2018). Furthermore, SIF is involved in the light reaction of photosynthesis (Gu, Han, Wood, Chang, & Sun, 2019), whereas V_{cmax} is involved in the dark reaction. As a result, the sensitivity of SIF to V_{cmax} is likely low (Frankenberg & Berry, 2018), which is revealed by both model simulation (van der Tol et al., 2016) and field observation (Yang et al., 2018).

The third category is mechanistic approaches. These approaches use optimality hypothesis to balance resource investments and carbon gains of plants. A typical theoretical framework uses an optimal nitrogen use hypothesis, assuming that plants optimize their nitrogen partitioning to maximize the photosynthetic carbon assimilation under specific environmental conditions and LNC (Ali et al., 2016). Another typical theoretical framework is based on coordination and co-optimization of Rubisco, light, and water costs for photosynthesis (Wang, Prentice, Keenan, et al., 2017). It hypothesizes that plants adjust nitrogen optimally in such a way that Rubisco- and electron transport-limited CO_2 assimilation rates are balanced (Chen, Reynolds, Harley, & Tenhunen, 1993) and operate stomata optimally in such a way that the summed unit costs of transpiration and carboxylation are minimized (Prentice, Dong, Gleason, Maire, & Wright, 2014). The combination of these two hypotheses yields a light use efficiency model from which V_{cmax} can be estimated (Bloomfield et al., 2018; Smith et al., 2019; Wang et al., 2020; Wang, Prentice, Davis, et al., 2017). The optimality theory suggests that environmental demand is the main driver of leaf nitrogen, whereas soil nitrogen supply is the main influence on aboveground canopy allocation. Therefore, unlike the nitrogen-partitioning model, the optimality-based model does not require information on LNC (which is unavailable at large scale) as an input and therefore is more suitable for diagnostic studies. Compared to statistical approaches, mechanistic approaches are less limited by the representativeness of calibration data and therefore are more robust for large-scale applications. Compared to inversion approaches, mechanistic approaches are not limited by GPP/SIF observations and therefore more general. Such mechanistic approaches have proven adept at predicting spatial variation in V_{cmax} (Smith et al., 2019), though their efficacy for predicting temporal changes remains largely untested.

V_{cmax} at a standardized temperature, for example, 25°C ($V_{cmax,25C}$), has considerable seasonal variation, similar to LNC and LCC (Wilson, Baldocchi, & Hanson, 2000, 2001). Ignoring the seasonality of $V_{cmax,25C}$ can lead to substantial errors in the estimation of carbon and water fluxes using TBMs (Kosugi, Shibata, & Kobashi, 2003; Luo et al., 2018). However, existing optimality-based models focus only on capturing global spatial and interannual variation of V_{cmax} and $V_{cmax,25C}$ under mean growing season environmental conditions (Bloomfield et al., 2018; Maire et al., 2012; Smith et al., 2019; Walker et al., 2017). To enable the prediction of seasonal variation in $V_{cmax,25C}$, further parameterization is needed.

The fundamental assumption of optimality-based models is that plants acclimate to the environment. In recent years, plant acclimation has been characterized by a legacy effect or ecological memory (i.e., the effect of the past on current and future plant and ecosystem functioning; Anderegg et al., 2015; Hughes et al., 2019; Ogle & Barber, 2016; Ogle et al., 2015). Ecological memory theory implies that antecedent environmental conditions have the potential to affect plant physiology, potentially including $V_{cmax,25C}$ (Fürstenau Togashi et al., 2018). Meanwhile, plants tend to co-vary canopy structure (particularly leaf area index, LAI, which determines the light absorption by plants) and functioning to acclimate to varying environmental conditions (i.e., canopy structure and functioning converge; Field, 1991). This functional convergence theory implies that canopy structure, which determines light absorption, carries

information on plant functioning and therefore has the potential to infer $V_{cmax,25C}$.

In this study, we proposed a pragmatic parameterization to enable an optimality-based model to capture the seasonality of C3 plant $V_{cmax,25C}$ benchmarked against field observations. We hypothesized that the consideration of the antecedent environment and dynamic light absorption will improve $V_{cmax,25C}$ estimation with regard to seasonal variation. To test this hypothesis and evaluate the model performance, we compiled an observational dataset of seasonal $V_{cmax,25C}$ from published data collected at 10 sites across diverse ecosystems.

2 | MODELING

2.1 | The optimality photosynthesis model

According to the mechanistic photosynthesis model proposed by Farquhar (Farquhar et al., 1980), the gross rate of CO_2 assimilation (A) is the lower of the Rubisco- or electron transport-limited rates. The optimality hypothesis posits that a leaf acclimates to prevailing environment, so that at a large timescale (e.g., a week, a month, or a growing season), A (g C m^{-2} day^{-1}) is close to the point where Rubisco-limited CO_2 assimilation rate (A_c) and electron transport-limited CO_2 assimilation rate (A_j) are equal (Haxeltine & Prentice, 1996; Keenan et al., 2016; Wang, Prentice, Keenan, et al., 2017):

$$A_c = V_{cmax}\frac{C_i-\Gamma^*}{C_i+K} = A_j = \frac{\alpha I}{\sqrt{1+\left(\frac{\alpha I}{J_{max}}\right)^2}}\frac{C_i-\Gamma^*}{4\left(C_i+2\Gamma^*\right)}, \tag{1}$$

where C_i (Pa) is the intercellular CO_2 concentration, Γ^* (Pa) is the CO_2 compensation point in the absence of dark respiration, K (Pa) is the Michaelis–Menten coefficient of Rubisco, α (g C/mol) is the intrinsic quantum yield of photosynthesis on an incident light basis, I (mol m^{-2} day^{-1}) is the incident photosynthetically active radiation (PAR), and J_{max} (μmol m^{-2} s^{-1}) is the maximum electron transport rate. Both K and Γ^* are functions of temperature (T; K), and their expression is provided in Table S1 (Bernacchi, Singsaas, Pimentel, Portis, & Long, 2001). Please note in some papers the intrinsic quantum yield and PAR are defined on an absorbed light basis, whereas here they are on an incident light basis. In addition, other forms of A_j exist, but the sensitivity of different forms is out of scope of this study.

The intrinsic quantum yield of photosynthesis α was initially considered constant at 1.02 g C/mol (Wang, Prentice, Keenan, et al., 2017) and was calculated by:

$$\alpha = \frac{a_L b_L}{k}\Phi_{PSII,max,dark}M, \tag{2}$$

where $a_L = 0.8$ is the leaf absorptance, $b_L = 0.5$ is the ratio of light captured by photosystem II to light absorbed by leaf, $k = 4$ is the number of electron equivalents required to reduce one molecule of CO_2, $\Phi_{PSII,max,dark} = 0.85$ is the maximum quantum yield of photosystem II for a typical dark-adapted leaf, and $M = 12$ is the weight in grams of 1 mol carbon. Under natural conditions, however, $\Phi_{PSII,max,dark}$ is only relevant when leaves begin photosynthesizing at dawn. Therefore, we replaced $\Phi_{PSII,max,dark}$ by the maximum quantum yield of photosystem II for a typical light-adapted leaf $\Phi_{PSII,max,light}$, which is a function of temperature (T; °C; Bernacchi, Pimentel, & Long, 2003; Stocker, Wang, et al., 2019; Wang et al., 2020):

$$\Phi_{PSII,max,light} = 0.352 + 0.022T - 0.00034T^2. \tag{3}$$

The optimality hypothesis also posits that plants adjust stomata to minimize the unit costs of transpiration (E) and carboxylation (V_{cmax}) relative to carbon assimilation (A; Prentice et al., 2014):

$$a\frac{\partial(E/A)}{\partial\chi} + b\frac{\partial\left(V_{cmax}/A\right)}{\partial\chi} = 0, \tag{4}$$

where χ (unitless) is the ratio of intercellular CO_2 (C_i) to ambient CO_2 (C_a; Pa), a and b are dimensionless cost factors for E and V_{cmax}, respectively. By applying Fick's law for diffusive transport to both transpiration and assimilation, χ can be solved from (4) as (Prentice et al., 2014):

$$\chi = \frac{\sqrt{\beta\frac{K+\Gamma^*}{1.6\eta^*}} + \frac{\Gamma^*\sqrt{D}}{C_a}}{\sqrt{\beta\frac{K+\Gamma^*}{1.6\eta^*}} + \sqrt{D}}, \tag{5}$$

where D (Pa) is the vapor pressure deficit (VPD), η^* is the viscosity of water relative to its value at 25°C, representing the effect of changing viscosity on the value of a at 25°C (Table S1). The ratio of cost factors for carboxylation and transpiration at 25°C $\beta = 240$ is fit from an isotope-derived χ database (Cornwell, 2017; Wang, Prentice, Keenan, et al., 2017).

The optimality hypothesis further assumes the existence of an optimal J_{max} that maximizes the differences between benefit (A_j) and cost ($c \times J_{max}$, where $c = 0.103$ is a dimensionless cost factor estimated according to the typical value of $J_{max}/V_{cmax} = 1.88$; Kattge & Knorr, 2007). V_{cmax} can therefore be solved from (1) as follows:

$$V_{cmax} = \varphi_0 I\frac{C_i-\Gamma^*}{C_i+2\Gamma^*}\sqrt{1-\left[\frac{4c\left(C_i+2\Gamma^*\right)}{C_i-\Gamma^*}\right]^{\frac{2}{3}}}. \tag{6}$$

Detailed deduction of this model can be found elsewhere (Smith et al., 2019; Wang et al., 2020; Wang, Prentice, Davis, et al., 2017; Wang, Prentice, Keenan, et al., 2017).

2.2 | Model parameterization for $V_{cmax,25C}$ seasonality

A total of five variables are involved in Equation (6): I, T, D, C_a, and surface pressure P_s to convert C_a, K, and Γ^* from concentration unit

(e.g., μmol/mol) to pressure unit (Pa). All of them refer to growing season or monthly mean values in existing optimality-based models (Bernotas et al., 2019; Bloomfield et al., 2018; Wang, Prentice, Keenan, et al., 2017).

As described in Section 2.1, leaf absorptance a_L is considered as a constant in existing optimality-based models; for example, 0.8 (Wang, Prentice, Keenan, et al., 2017), 0.5 (Bloomfield et al., 2018), and 0.79 (Smith et al., 2019) implied by a $\varphi = 0.257$ mol electrons mol photon^{-1} given an intrinsic quantum efficiency of 0.081 mol CO_2 mol photon^{-1} (Singsaas, Ort, & DeLucia, 2001) and 4 mol electrons are needed to produce 1 mol of CO_2. In reality, however, leaf absorptance varies over both space and time with varying pigments, water and dry matter contents, and leaf structure (Feret et al., 2008; Jacquemoud & Baret, 1990). Furthermore, the total interceptable light of a leaf is typically more than incident light due to multiple scattering effects within the canopy (Huang et al., 2007; Smolander & Stenberg, 2005; Zeng et al., 2019), and such effects vary with the dynamic canopy structure; this dynamic light absorption is not considered in existing optimality-based models.

To improve this incomplete assumption, we propose a four-step approach based on radiative transfer theory. First, we estimate the leaf area index (LAI) at the plant level (LAI_{plant}) from landscape-level ($LAI_{landscape}$) data (by either field measurements or satellite estimations) by accounting for the fraction of vegetation cover f_{plant} (by either field measurements or satellite estimations):

$$LAI_{plant} = LAI_{landscape}/f_{plant}. \tag{7}$$

Second, we estimate the plant-level F_{PAR} from LAI_{plant} by applying Beer's law:

$$F_{PAR} = \left(1-\rho_{PAR}\right)\left(1-e^{-k_d \Omega LAI_{plant}}\right), \tag{8}$$

where ρ_{PAR} is the PAR albedo, Ω is the clumping index, and k_d is the extinction coefficient under diffuse sky radiation (Goudriaan, 1977; Ryu, Lee, Jeon, Song, & Kimm, 2014):

$$k_d = -\frac{\ln\left[2\int_0^{\frac{\pi}{2}} e^{-0.5\Omega LAI_{plant}} \sin\theta\cos\theta d\theta\right]}{\Omega LAI_{plant}}, \tag{9}$$

where θ is the view zenith angle. Here, the diffuse extinction coefficient instead of direct one is used because the model calculates daily F_{PAR} instead of instantaneous F_{PAR}. ρ_{PAR} and Ω in Equation (8) are ideally plant-level values but practically landscape-level values given the availability of satellite estimations. The integration in Equation (9) can be solved using an exponential integral (Table S1). As the absorption of PAR is considered at the canopy level, leaf absorptance a_L in Equation (2) can be set to 1.

Third, we compute V_{cmax} (Equation 6) by replacing the constant value of a_L in Equation (2) with the spatiotemporally explicit F_{PAR} calculated from Equation (8). At this point, the derived V_{cmax} represents the plant-level averaged value ($V_{cmax,plant}$).

Finally, we convert the plant-averaged V_{cmax} (Equation 6) to top-leaf V_{cmax} ($V_{cmax,top\text{-}leaf}$; De Pury & Farquhar, 1997):

$$V_{cmax,top-leaf} = V_{cmax,plant}\frac{k_n}{1-e^{-k_n}}, \tag{10}$$

where k_n is a nitrogen distribution coefficient accounting for vertical variation in LNC within the plant canopy, and a larger k_n indicates a larger vertical variation in LNC and V_{cmax}. A mechanistic solution for k_n is unavailable, but meta-analysis studies have shown a negative relationship between k_n and LAI, and a positive relationship between k_n and clumping index (Hikosaka et al., 2016; Zhang, Hu, Hu, Fan, Zhou, & Tang, 2014). In this study, k_n is treated as a calibration parameter and we intend to seek for an empirical parameterization using LAI or clumping index. For simplicity, we use V_{cmax} to refer to $V_{cmax,top\text{-}leaf}$ hereafter to be consistent with existing optimality-based models.

In addition to the canopy structure, the antecedent environment is accounted for in this study. Specifically, values of I, T, D, C_a, P_s, and F_{PAR} averaged over the past n_{past} days are used as model inputs as analogs of the growing season mean or monthly mean values used in existing optimality-based models. Similar to k_n, a mechanistic solution for n_{past} is unavailable. Therefore, n_{past} is also treated as a calibration parameter in this study. Since studies have found that the length of lag varied region by region and such variation is likely to link with prevalent climate conditions (Ryan et al., 2015; Wu et al., 2015; Yang, Yang, & Merchant, 1997), we intend to seek for an empirical parameterization using PFT, mean annual temperature (MAT), or mean annual precipitation.

We further convert V_{cmax} to $V_{cmax,25C}$. This is necessary for two reasons. First, although V_{cmax} is considerably sensitive to temperature, V_{cmax} at a standardized temperature, usually at 25°C, correlates better to Rubisco content, LNC, and LCC (Houborg, McCabe, Cescatti, & Gitelson, 2015; Kattge et al., 2009). Second, using a standardized temperature allows for comparisons between different studies. A peaked Arrhenius equation $f(T)$ with temperature acclimation is used (Kattge & Knorr, 2007; Medlyn et al., 2002):

$$f(T_k) = e^{\frac{H_a(T_k-298)}{298RT_k}}\frac{1+e^{\frac{298\Delta S-H_d}{298R}}}{1+e^{\frac{T_k\Delta S-H_d}{T_kR}}}, \tag{11}$$

$$\Delta S = (-1.07t_{growth}+668.39)/1,000, \tag{12}$$

$$V_{cmax,25C} = \frac{V_{cmax}}{f(T_k)}, \tag{13}$$

where T_k is the temperature in Kelvin, $H_a = 72$ kJ/mol is the activation energy of V_{cmax}, $H_d = 200$ kJ/mol is the deactivation energy of V_{cmax}, ΔS (kJ mol^{-1} K^{-1}) is the entropy factor of V_{cmax}, t_{growth} is the average temperature from the preceding month (°C), and $R = 0.008314$ kJ mol^{-1} K^{-1} is the gas constant. Because $f(T_k)$ can be small at low temperatures and subsequently yields an unrealistically high $V_{cmax,25C}$ even with a very small V_{cmax}, we set a constraint of $f(T_k) \geq f(273.15) = 0.08$. Finally, a Savitzky–Golay filter is applied to the seasonal trajectory of the

estimated $V_{cmax,25C}$ to smooth the unrealistically large day-to-day variation caused by the temperature correction.

3 | MATERIALS AND METHODS

3.1 | Study sites and $V_{cmax,25C}$ measurements

To evaluate our model, we built an observational dataset of $V_{cmax,25C}$ by compiling independent data collected at 10 sites across diverse ecosystems covering six PFTs and seven climate zones (Table 1). These 10 sites were selected from the literature because (a) they were in flux tower stations, so meteorological observations were available; (b) field campaigns were conducted at least three times per growing season after 2001, so MODIS satellite observations were available; (c) leaf samples were collected from a sunlit canopy, so data approximately represented the TOC condition; (d) V_{cmax} values were fit from A–C_i curves obtained from gas exchange measurements; and (e) temperature corrections were applied and $V_{cmax,25C}$ values provided. For the SoyFACE site, only data collected from the reference site under natural conditions were used. Detailed descriptions of the 10 sites and data collection can be found in Method S1.

3.2 | Model inputs for $V_{cmax,25C}$ estimation

We prepared model inputs from both ground and satellite datasets at the 10 sites (Table 2). Because all 10 sites are located at flux tower stations, we acquired meteorological data, including incident PAR (I), air temperature (T_a), vapor pressure deficit (D), and surface pressure (P_s) from the FLUXNET2015 database (Pastorello et al., 2017), LaThuile2007 database (Agarwal et al., 2010), AmeriFlux database (Agarwal et al., 2010), EropeanFlux database (Sulkava, Luyssaert, Zaehle, & Papale, 2011), and KoFlux database (Kim, 2007). For sites which do not provide PAR directly, we converted incident shortwave radiation (SW) to PAR using the ratio of PAR to SW derived from Breathing Earth System Simulator (BESS) radiation products (Ryu, Jiang, Kobayashi, & Detto, 2018), which have provided daily 0.05° PAR/SW over the globe since 2000 using MODIS satellite data. We acquired the ambient CO_2 concentration (C_a) from either site observations or the ESA Climate Change Initiative Greenhouse Gas (GHG-CCI) product (Dils et al., 2014). GHG-CCI provides monthly 5° C_a over the globe from 2003 to 2015 using SCIAMACHY and GOSAT satellite data. We used outgoing PAR along with incident PAR from the flux tower datasets to calculate ρ_{PAR} when data are available, otherwise we used the "white-sky albedo for vis broadband" dataset from the MCD43A3 daily 500 m albedo product (Schaaf et al., 2002). We used field-measured LAI acquired by either LAI-2000 (LI-COR) or the destructive method if available; otherwise, we used the "Lai_500m" and "FparLai_QC" datasets from the MCD15A3H (since 2003) and MOD15A2H (before 2003) 4-day/8-day 500 m LAI/FPAR product (Myneni et al., 2002). We assumed that LAI-2000 data producers used the LI-COR software to process field measurements so that the reported LAI values were "quasi" actual LAI (Ryu et al., 2010), consistent with MODIS LAI. Woody LAI and background grass LAI were deducted when necessary. We treated the f_{plant} of woody plants and herbaceous plants in different manners. We assumed that woody plants have static tree cover

TABLE 1 Site information

Site	Year	Latitude	Longitude	Land cover	Climate zone	MAT (°C)	MAP (mm)	Reference
AU-Cum	2008 2009	−33.6152	150.7236	EBF	Cfa	17.3	850	Lin, Medlyn, De Kauwe, and Ellsworth (2013)
BR-Sa1	2012 2013 2014	−2.8567	−54.9589	EBF	Am	26.1	2,075	Albert et al. (2018)
CA-Cbo	2014	44.3167	−79.9333	DBF	Dfb	6.7	876	Croft et al. (2017)
FI-Hyy	2011	61.8474	24.2948	ENF	Dfc	3.8	709	Kolari et al. (2014)
IT-Non	2003	44.6898	11.0887	MF	Cfa	14.5	1,000	Grassi, Vicinelli, Ponti, Cantoni, and Magnani (2005)
JP-TKY	2004	36.1461	137.4231	DBF	Dfb	6.5	2,275	Muraoka et al. (2010)
KR-CRK	2016	37.1597	127.6536	CRO	Dwa	10.2	1,394	Hwang et al. (2020)
SoyFACE	2001	40.0340	−88.2333	CRO	Dfa	11.0	991	Bernacchi, Morgan, Ort, and Long (2005)
US-Ha1	2010	42.5378	−72.1715	DBF	Dfb	6.6	1,071	Dillen, de Beeck, Hufkens, Buonanduci, and Phillips (2012)
US-Ton	2001	38.4316	−120.9660	WSA	Csa	15.8	559	Xu and Baldocchi (2003)

Abbreviations: Am, tropical monsoon climate; Cfa, humid subtropical climate; CRO, cropland; Csa, hot summer Mediterranean climate; DBF, deciduous broadleaf forest; Dfa, hot summer humid continental climate; Dfb, warm summer humid continental climate; Dfc, subarctic climate; Dwa, monsoon-influenced hot summer humid continental climate; EBF, evergreen broadleaf forest; ENF, evergreen needleleaf forest; MAP, mean annual precipitation; MAT, mean annual temperature; MF, mixed forest; WSA, woody savanna.

TABLE 2 Data sources of model inputs. Site observations were used when available, but all can be replaced by global datasets provided by gridded climate or satellite products. Please refer to Method S2 for details

Site	Meteorology (I, T_a, D, P_s)	PAR/SW	C_a	ρ_{PAR}	$LAI_{landscape}$	f_{plant}	Ω
AU-Cum	FLUXNET	BESS	FLUXNET	MCD43A3	MCD15A3H (max: 2.1)	MOD44B (0.33)	MODIS (0.81)
BR-Sa1	FLUXNET	FLUXNET	FLUXNET	FLUXNET	LAI-2000 (max: 4.9)	Camera (max: 0.98)	MODIS (0.51)
CA-Cbo	AmeriFlux	AmeriFlux	AmeriFlux	AmeriFlux	LAI-2000 (max: 4.4)	MOD44B (0.87)	MODIS (0.71)
FI-Hyy	FLUXNET	FLUXNET	FLUXNET	FLUXNET	LAI-2000 (max: 2.2)	MOD44B (0.53)	MODIS (0.55)
IT-Non	EropeanFlux	BESS	GHG-CCI	MCD43A3	MCD15A3H (max: 2.7)	MOD44B (0.77)	MODIS (0.77)
JP-TKY	LaThuile	LaThuile	LaThuile	LaThuile	Destructive (max: 4.9)	MOD44B (0.72)	MODIS (0.51)
KR-CRK	AsiaFlux	AsiaFlux	GHG-CCI	MCD43A3	Destructive (max: 5.9)	From LAI (max: 0.95)	MODIS (0.78)
SoyFACE	AmeriFlux	BESS	GHG-CCI	MCD43A3	MOD15A2H (max: 6.2)	From LAI (max: 0.95)	MODIS (0.77)
US-Ha1	FLUXNET	FLUXNET	FLUXNET	MCD43A3	LAI-2000 (max: 3.0)	MOD44B (0.61)	MODIS (0.66)
US-Ton	FLUXNET	FLUXNET	FLUXNET	FLUXNET	MOD15A2H and destructive LAI of grass (max: 1.6)	LiDAR (0.45)	MODIS (0.80)

TABLE 3 A list of experiment configurations

Configuration	Dynamic light absorption	Antecedent environment	Purpose
#1	Site-specific k_n	Site-specific n_{past}	The best model performance
#2	Estimated k_n	Estimated n_{past}	The scalable solution
#3	Constant k_n	Estimated n_{past}	Importance of varying k_n
#4	Estimated k_n	Constant	Importance of varying n_{past}
#5	Not considered but use $a_L = 0.8$	Estimated n_{past}	Importance of canopy structure
#6	Estimated k_n	Not considered but use monthly mean	Importance of antecedent environment
#7	Not considered but use $a_L = 0.8$	Not considered but use monthly mean	The original optimality-based model

in a specific year. We used tree cover derived from tower camera, terrestrial LiDAR, or the "Percent_Tree_Cover" datasets from the MOD44B yearly 250 m Vegetation Continuous Fields product (Hansen et al., 2003). In the case of herbaceous plants, we assumed that they develop their canopy cover dynamically. We calculated f_{plant} using Beer's law in the nadir direction:

$$f_{plant} = 1 - e^{-0.5\Omega LAI_{landscape}}, \quad (14)$$

where $LAI_{landscape}$ was acquired from field measurements or satellite estimations, and Ω was from a global 500 m clumping index product derived from the MODIS dataset (Wei, Fang, Schaaf, He, & Chen, 2019). The data are provided in 8 day intervals from 2001 to 2017. Considering data noise and data gaps, we only used annual mean values of Ω. Detailed descriptions of the data processing at the 10 sites can be found in Method S2.

3.3 | Experiments and evaluation

To test our hypothesis that considering the antecedent environment and dynamic light absorption will improve $V_{cmax,25C}$ estimation with regard to seasonal variation, we conducted experiments using seven configurations (Table 3). First, we calibrated the two model parameters, k_n and n_{past}, for each site by minimizing the root mean square error (RMSE) between the measured and estimated

$V_{cmax,25C}$. This configuration refers to the best model performance. Second, we compared calibrated k_n with growing season mean LAI and clumping index to build an empirical parameterization for k_n, and compared calibrated n_{past} with MAT and MAP to build an empirical parameterization for n_{past}. The empirically estimated k_n and n_{past} were subsequently used to estimate $V_{cmax,25C}$. Compared to the first configuration, we expected this to have the potential to be scaled up for global $V_{cmax,25C}$ estimation because it avoids site-specific parameter values. For the third configuration, we calculated the median value of site-specific k_n as a global constant, but kept the empirically estimated n_{past} in configuration #2. For the fourth configuration, we calculated the median value of site-specific n_{past} as a global constant, but kept the empirically estimated k_n in configuration #2. Compared to #2, configurations #3 and #4 were to investigate the importance of using the empirically estimated k_n and n_{past}, respectively. For the fifth configuration, we used a fixed leaf absorptance $a_L = 0.8$ to calculate the intrinsic quantum yield of photosynthesis (Equation 2) instead of canopy absorptance F_{PAR} considering the canopy structure, but kept the empirically estimated n_{past} in configuration #2. Correspondingly, for the sixth configuration, we used monthly mean environmental data as model forcing without considering the antecedent environment, but kept the empirically estimated k_n in configuration #2. Compared to #2, configurations #6 and #7 were to investigate the importance of considering the dynamic light absorption and antecedent environment, respectively, in accounting for the $V_{cmax,25C}$ seasonality. Finally, we used the original optimality-based model (using a fixed leaf absorptance $a_L = 0.8$ and monthly mean environmental data) as a baseline to investigate the overall improvement of the proposed model parameterization (configuration #2). For each configuration, we calculated coefficient of determination (R^2), RMSE, and mean bias error (bias) at each site for quantitative performance assessment.

4 | RESULTS

4.1 | Seasonal variation in $V_{cmax,25C}$ and model calibration

The field measurements of maximum carboxylation rate of top leaf at 25°C leaf temperature ($V_{cmax,25C}$) show significant seasonal variation across the 10 study sites (Figure 1). Seasonal variation differs among the individual sites. Four of the 10 sites (IT-Non, KR-CRK, SoyFACE, and US-Ha1) display peak $V_{cmax,25C}$ values in early summer (June). Two sites (AU-Cum and US-Ton) display peak $V_{cmax,25C}$ values in late spring (November for AU-Cum and May for US-Ton). The other four sites display peak V_{cmax} values in high summer (July for FI-Fyy), late summer (August for JP-TKY), early autumn (September for CA-Cbo), and the late dry season (October–December for BR-Sa1). The highest $V_{cmax,25C}$ value (120 μmol m^{-2} s^{-1}) is found at the crop site KR-CRK, followed by the other crop site SoyFACE and the woody savanna site US-Ton. Temperate forest sites generally show medium peak V_{cmax}

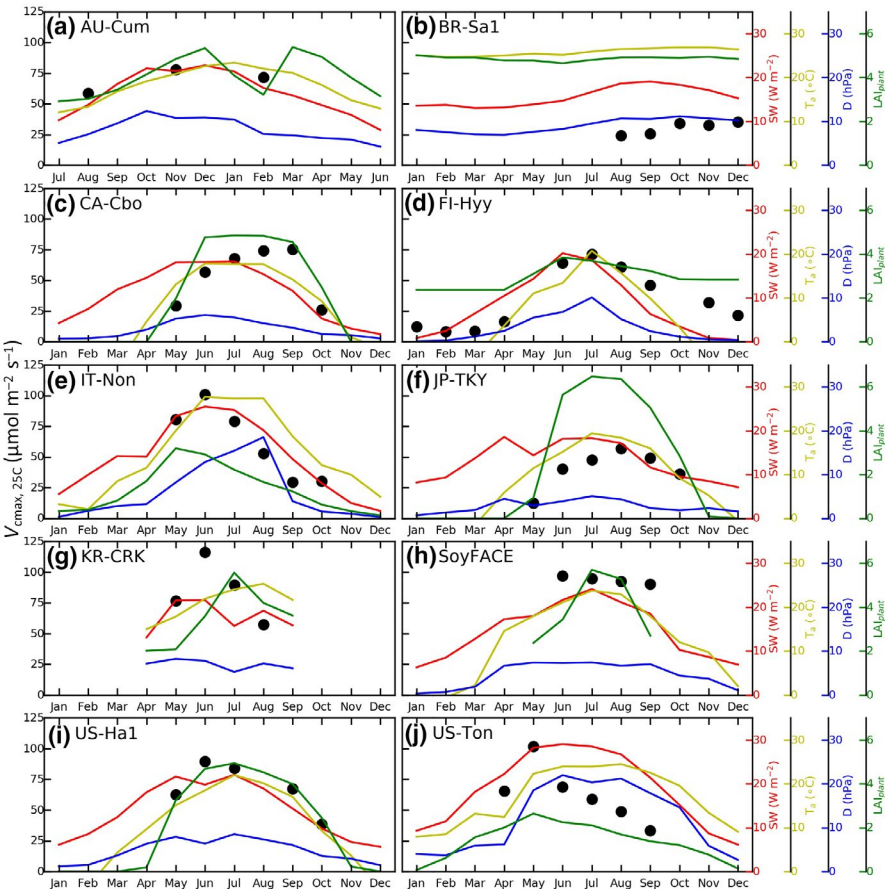

FIGURE 1 Monthly mean measured $V_{cmax,25C}$, incident shortwave radiation (SW), air temperature (T_a), vapor pressure deficit (D), and leaf area index at the plant level (LAI_{plant}) at the 10 study sites (a–j; Table 1) [Colour figure can be viewed at wileyonlinelibrary.com]

values (60–100 μmol m^{-2} s^{-1}), whereas the lowest peak $V_{cmax,25C}$ value (~40 μmol m^{-2} s^{-1}) is found at the tropical forest site BR-Sa1.

By fitting the newly parameterized optimality-based model (Section 2.2) with field-measured $V_{cmax,25C}$ site by site, the two model parameters, k_n and n_{past}, were obtained for each site (Figure 2). Across all the 10 sites, the median values of k_n and n_{past} are 0.35 and 40, respectively. Clear PFT dependence can be observed for both parameters. The median values of k_n follow the order evergreen (0.10) < deciduous (0.44) < crops (1.16), whereas the median values of n_{past} follow the order evergreen (134) > deciduous (39) > crops (15). Furthermore, both parameters have proxies. Overall, k_n negatively correlates with the growing season mean LAI at the plant level (L_{GS}; Figure 2a) and positively correlates with the clumping index (Ω; Figure S8a). Excluding two crop sites, a logarithmic function can be fit from the k_n ~ L_{GS} relationship (R^2 = .75) by:

$$k_n = -0.62\log(L_{GS}) + 0.98. \quad (15)$$

A non-monotonic relationship is shown between n_{past} and MAT (Figure 2b), that n_{past} first decreases as MAT increases, and then increases with MAT. The inflection point appears around MAT = 12°C. The n_{past} ~ MAT relationship can be fit by a quadratic function (R^2 = .77):

$$n_{past} = 0.82\mathrm{MAT}^2 - 19.52\mathrm{MAT} + 146.14. \quad (16)$$

No correlation between n_{past} and MAP is shown (Figure S8b). Consequently, we used Equation (15) to empirically estimate k_n for non-crop sites in configurations #2, #4, and #6, and used the mean value of k_n = 1.16 for the crop sites. We used Equation (16) to empirically estimate n_{past} for all sites in configurations #2, #3, and #5. We used the global constant k_n = 0.35 and n_{past} = 40 in configurations #3 and #4, respectively.

4.2 | Performance of the optimality-based model in estimating $V_{cmax,25C}$

In general, $V_{cmax,25C}$ estimations by the newly parameterized optimality-based model with k_n and n_{past} calibrated site by site (configuration #1) agree fairly well with the field measurements (Figures 3 and 4; Figure S1). The median R^2 and RMSE values between field measurements and model estimations across the 10 sites are 0.83 and 11.2 μmol m^{-2} s^{-1}, respectively. Relatively high R^2 values (>.60) are found at eight of the 10 sites, whereas the other two sites, BR-Sa1 and SoyFACE, are characterized by small seasonal variations of $V_{cmax,25C}$ (coefficient of variation < 30%). None of the 10 sites has an RMSE value larger than 20 μmol m^{-2} s^{-1}, which suggests robust model performance.

The scalable solution (configuration #2), using empirically estimated k_n (Equation 15) and n_{past} (Equation 16), provides almost identical results with the site-specific model (configuration #2) at most sites (Figures 3 and 4; Figure S2). The median R^2 and RMSE values between field measurements and model estimations across the 10 sites are 0.81 (0.83 for configuration #1) and 11.7 (11.2 for configuration #1) μmol m^{-2} s^{-1}, respectively. Except for the two sites with small seasonal variations of $V_{cmax,25C}$ (BR-Sa1 and SoyFACE), all other sites achieve R^2 > .70. Same with configuration #1, none of the 10 sites has an RMSE value larger than 20 μmol m^{-2} s^{-1}, which suggests robust model performance. When all of the 10 sites data are combined together for the evaluation, the scalable solution explains 78% seasonal and spatial variations in field-measured $V_{cmax,25C}$ (Figure 5a).

In contrast, the original optimality-based model without the consideration of canopy structure and antecedent environment effects (configuration #7) disagrees with the field measurements (Figures 3 and 4; Figure S7). The median R^2 and RMSE values between field measurements and model estimations across the 10 sites are 0.15 (0.68 smaller than #1) and 21.2 μmol m^{-2} s^{-1} (10.0 μmol m^{-2} s^{-1} larger than #1), respectively. None of the 10 sites has an R^2 value larger than .6. High RMSE values (>20 μmol m^{-2} s^{-1}) are found at six of the 10 sites. When all data are combined together for the evaluation, the original optimality-based model only explains 35% seasonal and spatial variations in field-measured $V_{cmax,25C}$ (Figure 5b). In particular, most simulation are within a narrow range (30–80 μmol m^{-2} s^{-1}), leading to a pattern of overestimation in the low value part and underestimation in the high value part.

The difference between configurations #2 and #3 (Figure S3) is that the former one employs empirically estimated k_n (Figure 2a), while the later one uses a global constant k_n (0.35). Therefore, the

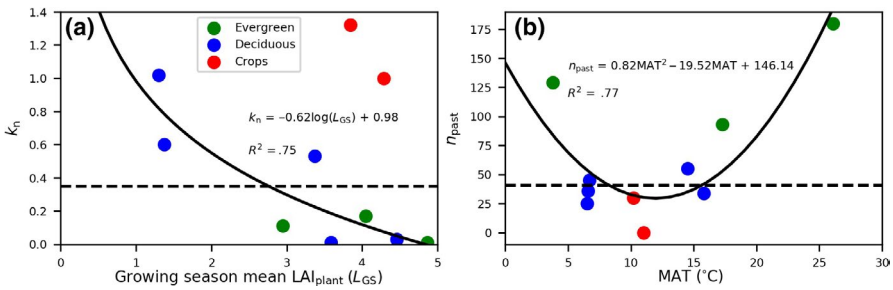

FIGURE 2 Parameterization of the two model parameters, k_n and n_{past}. (a) k_n as a logarithmic function of the growing season mean LAI at the plant level (L_{GS}), excluding crop. (b) n_{past} as a quadratic function of the MAT. k_n and n_{past} are obtained by site-by-site calibration of the optimality-based model. The solid curves are empirical functions fit from dots. The dash lines are the median k_n and n_{past} of the 10 sites [Colour figure can be viewed at wileyonlinelibrary.com]

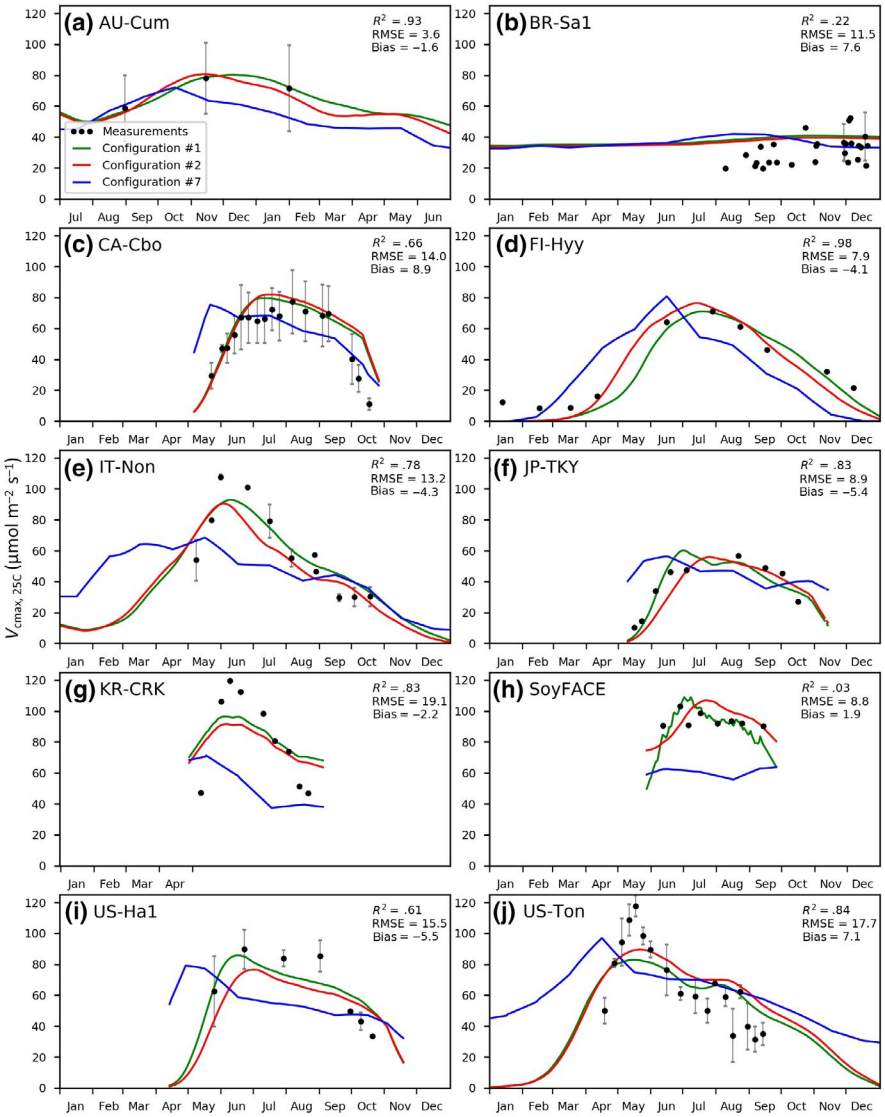

FIGURE 3 Comparison of daily $V_{cmax,25C}$ between field measurements and model estimations at the 10 study sites (a–j). Configuration #1 refers to the best model performance with site-specific k_n and n_{past}. Configuration #2 refers to the scalable solution with empirically estimated k_n and n_{past}. Configuration #7 refers to the original optimality-based model without the consideration of dynamic light absorption and antecedent environment. R^2, root mean square error, and bias values are for configuration #2 [Colour figure can be viewed at wileyonlinelibrary.com]

comparison between these two configurations indicates the importance of using the empirically estimated k_n. It is observed that the R^2 values are the same between configurations #2 and #3 for each site (Figure 4), which indicates that the value of k_n does not influence the seasonal pattern of the estimated $V_{cmax,25C}$. This is because k_n plays a role in converting plant-averaged V_{cmax} into top-leaf V_{cmax} (Equation 10), and it only influences the magnitude of the estimated $V_{cmax,25C}$. As a result, configuration #3 without an accurate quantification of k_n cannot provide accurate estimation of $V_{cmax,25C}$ with regard to the magnitude, which is revealed by higher RMSE values compared to configuration #2 (Figure 4). In addition, the magnitude is related to the spatial variation. When spatial and seasonal variations are evaluated together ("all sites" in Figure 5), configuration #3 (0.62) yields much lower R^2 than configuration #2 (0.78).

The difference between configurations #2 and #4 (Figure 6) is that the former one employs the empirically estimated n_{past} (Figure 2b), while the later one uses a global constant n_{past} (40). Therefore, the comparison between these two configurations indicates the importance of using the empirically estimated n_{past}. Although the R^2 values differ for individual sites, which indicate that n_{past} influences the seasonal pattern of the estimated $V_{cmax,25C}$, the median R^2 of configuration #4 (0.83) is even slightly higher than configuration #2 (0.81). Similarly, the differences in RMSE are also small, generally less than 2.0 μmol m^{-2} s^{-1} except for FI-Hyy (3.6 μmol m^{-2} s^{-1}). This is because n_{past} values of most sites are generally located around the median value (Figure 2b). BR-Sa1, AU-Cum, and SoyFACE deviate from the median n_{past}, but these sites are characterized by small seasonality of the field-measured $V_{cmax,25C}$, and therefore, even large differences in n_{past} do not lead to large differences in RMSE of the estimated $V_{cmax,25C}$. When spatial and seasonal variations are evaluated together ("all sites" in Figure 4), configuration #4 (0.77 and 13.5 μmol m^{-2} s^{-1}) only yields slightly lower R^2 and higher RMSE than configuration #2 (0.78 and 13.1 μmol m^{-2} s^{-1}).

The difference between configurations #2 and #5 (Figure S5) is that the former accurately accounts for the canopy structure effects on light absorption, while the latter uses a constant leaf absorptance

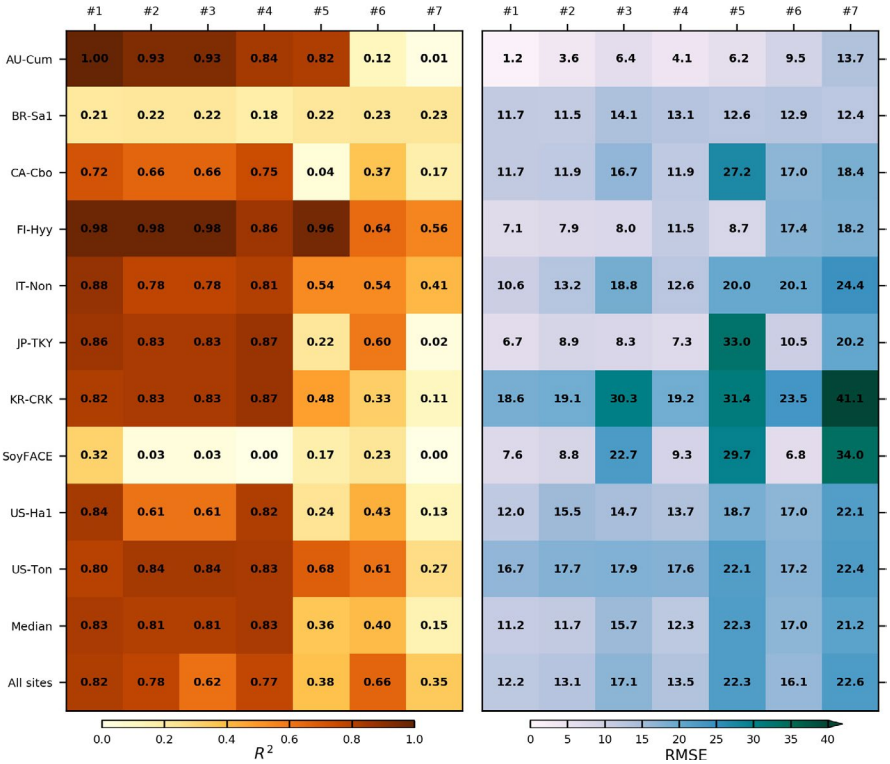

FIGURE 4 Performance of the optimality-based model at different sites (*y*-axis) with different configurations (*x*-axis). The simulation R^2 and root mean square error (RMSE) values are shown in the left and right panels, respectively. See Table 1 for the information of the 10 sites. The item "median" means median values of the 10 sites, which indicates the overall model performance of capturing the seasonal variation in $V_{cmax,25C}$. The item "all sites" means all data from the 10 sites combined, which indicates the overall model performance of capturing both seasonal and spatial variations in $V_{cmax,25C}$. See Table 3 for the information of the seven configurations [Colour figure can be viewed at wileyonlinelibrary.com]

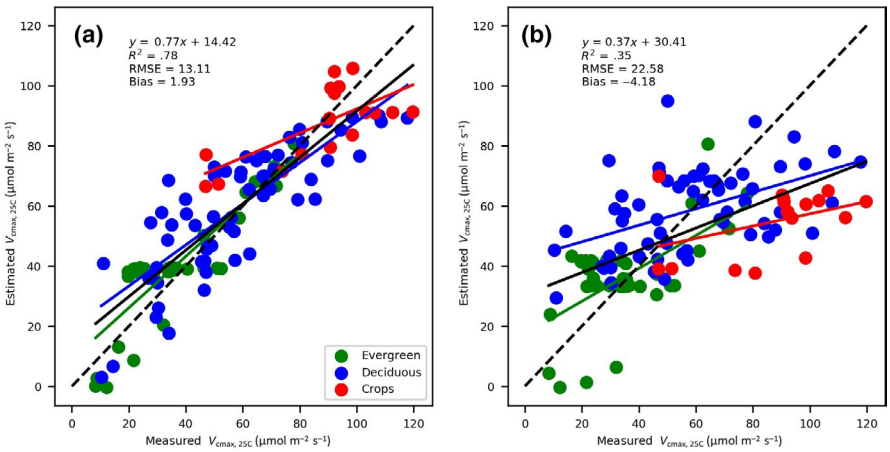

FIGURE 5 Scatterplot of daily $V_{cmax,25C}$ between field measurements and model estimations with (a) the scalable parameterization solution (configuration #2) and (b) the original optimality-based model (configuration #7) [Colour figure can be viewed at wileyonlinelibrary.com]

a_L = 0.8. Therefore, the comparison between these two configurations indicates the importance of considering the dynamic light absorption. Figure 4 reveals the substantial difference in both R^2 and RMSE. Configuration #5 can only explain 36% seasonal variation and 38% seasonal and spatial variations in $V_{cmax,25C}$, and yields about 11 μmol m^{-2} s^{-1} larger RMSE than configuration #2.

The difference between configurations #2 and #6 (Figure S6) is that the former uses antecedent environment, while the latter uses monthly mean environment. Therefore, the comparison between these two configurations indicates the importance of considering the antecedent environment. Figure 4 reveals the substantial difference in both R^2 and RMSE. Configuration #6 can only explain 40% seasonal variation and 66% seasonal and spatial variations in $V_{cmax,25C}$, and yields about 5 μmol m^{-2} s^{-1} larger RMSE than configuration #2.

5 | DISCUSSION

5.1 | Efficacy of the model parameterization

Using the new parameterization in this study, the optimality-based model can produce reasonable estimates of daily $V_{cmax,25C}$ against field measurements across the 10 sites (Figure 3). A comparison between seven experiment configurations (Figure 4) supports our hypothesis: considering the antecedent environment and dynamic light absorption improves $V_{cmax,25C}$ estimation with regard to seasonal variation. Benchmarked with configuration #2 (using empirically estimated k_n and n_{past}), when the antecedent environment (#6) or dynamic light absorption (#5) is not considered, the median RMSE between field measurements and model estimations across the 10 sites increases by 45% and 91%, respectively. While the importance

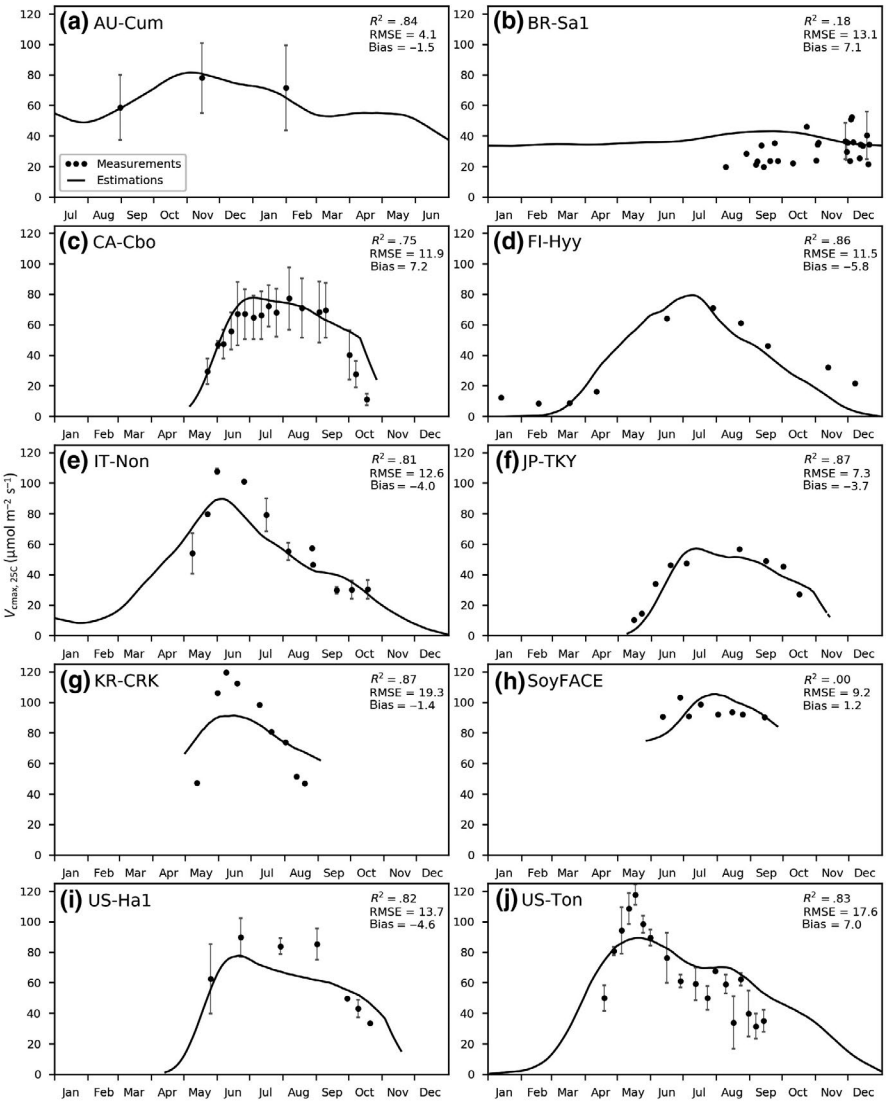

FIGURE 6 Comparison of daily $V_{cmax,25C}$ between field measurements and model estimations (configuration #4) at the 10 study sites (a–j). Configuration #4 refers to a scalable solution with empirically estimated k_n (Equation 15) and globally constant n_{past} (40)

of incorporating the antecedent environment into $V_{cmax,25C}$ modeling corroborates that plants dynamically acclimate to the past environment with ecological memory, the importance of incorporating the dynamic light absorption is in accordance with the functional convergence theory, which suggests that plants change canopy structure and leaf pigments by the availability of resources as a result of evolutionary processes to optimize carbon fixation (Goetz, Prince, Goward, Thawley, & Small, 1999). This actually forms the basis of the light use efficiency concept widely used by the remote-sensing community (Hilker, Coops, Wulder, Black, & Guy, 2008; Medlyn, 1998; Monteith, 1972, 1977; Running et al., 2004).

Site-by-site calibration yields a PFT dependence for the parameter k_n (Figure 2a). The order of evergreen < deciduous < crops is in line with a meta-analysis study (Zhang, Guanter, et al., 2014). Relatively small k_n values for evergreen forest have also been reported by other studies. For example, k_n measurements in the Amazon forest show an exponential relationship with top-leaf $V_{cmax,25C}$ (Lloyd et al., 2010): $k_n = \exp(0.00963 \times V_{cmax,25C} - 2.43)$. When $V_{cmax,25C}$ = 40 μmol m^{-2} s^{-1}, k_n = 0.13, similar to our calibrated k_n for evergreen forests (0.10). By contrast, relatively large k_n values for crops have also been reported, for example, 0.713 (De Pury & Farquhar, 1997), 1.01 (Bertheloot, Martre, & Andrieu, 2008), and 1.05 (Lemaire, Onillon, Gosse, Chartier, & Allirand, 1991), in line with our result (k_n = 1.18). By comparison, moderate k_n values have been reported for other PFTs, for example, 0.3 (Kitao et al., 2018), 0.41 (Jongschaap & Booij, 2004), 0.5 (Walker et al., 2018), and 0.2–0.5 (Anten, Werger, & Medina, 1998), which justify our k_n (0.48) for deciduous forest, mixed forest, and savanna. The median k_n of the 10 sites is 0.35, which agrees well with a meta-analysis reporting a $k_n = 0.41 \pm 0.35$ over a wide range of literature (Hikosaka et al., 2016). Such PFT-dependent k_n can be partly attributed to canopy structure. Our findings that k_n negatively correlates with plant-level LAI (Figure 2a) and positively correlates with clumping index (Figure S8a) are consistent with two meta-analysis studies (Hikosaka et al., 2016; Zhang, Guanter, et al., 2014). There are two potential reasons. On the one hand, the negative k_n ~ LAI relationship is likely related to the nitrogen availability. A higher k_n means most nitrogen are concentrated in the upper canopy, then LAI should be low as there is no reason to hold so many leaves without nitrogen in the lower canopy. On

the other hand, a clumped canopy (small Ω) allows more light to penetrate into the lower part of the canopy, inducing less vertical variation in light and thus nitrogen (small k_n).

Compared to k_n, the other calibrated parameter, n_{past}, might be more empirical. Site-by-site calibration indicates that evergreen forests had the largest n_{past} (~4 months), followed by deciduous ecosystems (~1.5 months) and crops (~0.5 months). This may indicate that forests respond more to long-term variation in the environment, whereas crops are more responsive to short-term changes. One relevant study (Bunting, Munson, & Villarreal, 2017) also reveals that woodland communities have stronger relationships with the climate at long lags (e.g., 6 months) than herbaceous communities. Nevertheless, other studies have reported considerably divergent legacy effects varying with plant traits and environmental drivers (Guo & Ogle, 2019; Kropp et al., 2017; Liu, Schwalm, Samuels-Crow, & Ogle, 2019). It is possible that the n_{past} difference in PFT is due to artificial factors. For example, we use the same n_{past} for all six inputs (I, T, D, C_a, P_s, and F_{PAR}), which may be parsimonious and difficult to interpret. In addition, evergreen forests in our study have longer seasonal data records than crops (Figure 4), which likely influence calculation of the antecedent environment. The quadratic n_{past} ~ MAT relationship suggests plants living in hot and cold climates need longer time to acclimate or have better memory than those living in warm climates. However, more evidence are warranted to support this pattern. Consequently, it might be more solid to use a global constant n_{past} (40 days; median of the 10 sites) in the model instead of empirically estimated n_{past}. This configuration (#4) yields reasonable seasonal variation in $V_{cmax,25C}$ (Figure 6) without much accuracy loss compared to configuration #2 (Figure 5). The n_{past} = 40 as a constant is comparable with other studies of legacy effects of gross primary production (3 months; Coops, Jassal, Leuning, Black, & Morgenstern, 2007; Leuning, Cleugh, Zegelin, & Hughes, 2005) and light use efficiency (1–2 months; Zhang et al., 2015). The success of this parameterization strategy further indicates plants gradually change their functions to optimize resource exploration and highlights the need to develop a mechanistic model of legacy effects or ecological memory. We therefore consider configuration #4 (an empirically estimated k_n and a constant n_{past}) as the final SVOM.

5.2 | Limitations

The optimality-based model does not explicitly include soil moisture effects. Water stress is k_n own as a major factor that reduces $V_{cmax,25C}$ (Wilson, Baldocchi, & Hanson, 2000; Xu & Baldocchi, 2003). Our model is able to partially capture seasonal variation at the dry ecosystem site US-Ton and a mesic site IT-Non experiencing drought (Figure 4). There are possibly two reasons, first severe water stress is reflected in LAI and albedo data, which in turn propagate to $V_{cmax,25C}$ because plants reallocate nitrogen resource to match reduced APAR (Xu & Baldocchi, 2003). Second, severe drought is usually associated with a heat wave, which has a substantial negative impact on $V_{cmax,25C}$ estimations via the temperature correction (Fürstenau Togashi et al., 2018). However, it is also observed that our model yields less decline in $V_{cmax,25C}$ during the dry-down period at these two sites. To date, how soil moisture influences $V_{cmax,25C}$ remains unclear (Flexas et al., 2006). In particular, whether light to moderate water stress, which may not be severe enough to dramatically reduce LAI, can reduce $V_{cmax,25C}$ warrants further investigation. Although efforts have been made to develop water stress functions for $V_{cmax,25C}$ (Keenan, Sabate, & Gracia, 2010), most are empirical and thus are not incorporated into our mechanistic model to avoid over-tuning. Recent studies have indicated that parameterizing the cost ratio β (Equation 5), which varies over time as a result of varying water potential between soil and leaves, is a potential pathway to incorporate the soil moisture effect into the optimality model (Lavergne et al., 2020; Stocker, Wang, et al., 2019).

Another limitation is that the leaf age effect is not parameterized in the model for evergreen forests. Field measurements in the Amazon forest have shown that mature leaves tend to have higher V_{cmax} values than young and old leaves (Wu et al., 2016). Field measurements in a montane temperate forest have also displayed different seasonal trajectories of Rubisco content for leaves of different ages (Katahata, Naramoto, Kakubari, & Mukai, 2007). However, studies on these mechanisms are still ongoing, and little data are available for a general parameterization.

5.3 | Global implications

Recently, two global $V_{cmax,25C}$ datasets have been derived using remote sensing data. One is based on the statistical approach (Alton, 2018). Empirical relationships are built between MERIS Terrestrial Chlorophyll Index (MTCI) and LCC, between LCC and maximum electron transport rate at 25°C ($J_{max,25C}$), and between $J_{max,25C}$ and $V_{cmax,25C}$. The other is based on the inversion approach (He et al., 2019). Empirical relationships are built between SIF and GPP for different PFTs, and the SIF-derived GPP is used to assimilate a TBM to retrieve $V_{cmax,25C}$. Both datasets provide seasonally varying $V_{cmax,25C}$, yet they have not been evaluated against field measurements of seasonal $V_{cmax,25C}$.

The optimality-based model has a great potential to provide a satellite-derived $V_{cmax,25C}$ through another pathway, the mechanistic approach. Model inputs related to canopy structure, including LAI, clumping index, fraction of vegetation cover, and PAR albedo, are all available at fine spatial resolution (e.g., 500 m) globally. Two key environmental forcing, PAR and CO_2 concentration, are also globally available from satellite data (Jiang & Ryu, 2016). Intercomparison of $V_{cmax,25C}$ estimations between these three distinct approaches may better constrain the spatial and temporal variations of global $V_{cmax,25C}$, and further improve global GPP estimation. It could also provide insight to the theory by examining when and where plants diverge from optimality.

The TBM community has focused on the relationship between LNC and $V_{cmax,25C}$. Those models consider LNC a key variable

because Rubisco is composed of a large amount of nitrogen (Walker et al., 2014). However, it is difficult to estimate LNC mechanically and the proportion of LNC used for $V_{cmax,25C}$ spatially and temporally (Ali et al., 2016). As a result, nitrogen-based TBMs do not predict reasonable spatial patterns at global scales (Walker et al., 2017), and their performance for seasonal variation in $V_{cmax,25C}$ has not been evaluated to date.

Our study provides a pathway for improving $V_{cmax,25C}$ modeling in TBMs. Although we consider LNC–$V_{cmax,25C}$ relationship a bottom-up approach, the optimality-based model based on plant evolutionary strategy can be considered a top-down approach. Such a model is independent of the nitrogen cycle but produces overall reliable estimates of $V_{cmax,25C}$ at a daily scale. A possible explanation for this is that photosynthetic demand drives LNC, rather than the other way around (Dong et al., 2017; Evans, 1989; Smith et al., 2019). Although we used canopy structure data from field measurements and satellite observations in this study, we suggest that the optimality-based model can be integrated into TBMs without any satellite data, so long as the host TBM can simulate vegetation dynamics.

To summarize, we have developed a new parameterization scheme to enable the optimality-based model to simulate seasonal variation in C3 plant photosynthetic capacity. The new parameterization considers the antecedent environment and dynamic light absorption, and it is independent from PFT. The agreement between field measured seasonal $V_{cmax,25C}$ data and optimality-based model-estimated daily $V_{cmax,25C}$ at 10 sites suggests the ability of plants to acclimate to environmental conditions. Such efficient resource utilization may help plants survive and evolve in the context of global climate change. This study also supports the notion of the existence of a universal model with a solid theoretical basis that can predict photosynthetic behavior at global scale (Wang, Prentice, Keenan, et al., 2017).

ACKNOWLEDGEMENTS

This research was conducted with support of the Korea Environment Industry & Technology Institute (KEITI) through its Urban Ecological Health Promotion Technology Development Project funded by the Korea Ministry of Environment (MOE) (2019002760002), and supported by the National Research Foundation of Korea (NRF-2016M1A5A1901789, NRF-2019R1A2C2084626). T.F.K. was supported by the NASA Terrestrial Ecology Program IDS Award NNH17AE86I. We thank Drs. Nicholas Smith, Benjamin Stocker, Colin Prentice, and Jingming Chen for the discussion of the optimality theory. All the field measured $V_{cmax,25C}$ data used in this manuscript were collected from literature and we appreciate those authors for publishing their data. English proofread was supported by Research Institute of Agriculture and Life Sciences at Seoul National University.

CONFLICT OF INTEREST

The authors declare no conflict of interest.

AUTHOR CONTRIBUTION

C.J. and Y.R. designed the study. C.J. developed the model, carried out all the analyses, constructed the figures and tables, and wrote the first draft. All authors contributed to the improvement of the model, the interpretation of the results, and the refinement of the text.

DATA AVAILABILITY STATEMENT

The codes of the proposed Seasonal V_{cmax} Optimality Model (SVOM) and all data used in this study are available at https://github.com/chongya/SVOM.

ORCID

Chongya Jiang https://orcid.org/0000-0002-1660-7320
Youngryel Ryu https://orcid.org/0000-0001-6238-2479
Han Wang https://orcid.org/0000-0003-2482-1818
Trevor F. Keenan https://orcid.org/0000-0002-3347-0258

REFERENCES

Agarwal, D. A., Humphrey, M., Beekwilder, N. F., Jackson, K. R., Goode, M. M., & Van Ingen, C. (2010). A data-centered collaboration portal to support global carbon-flux analysis. *Concurrency Computation Practice and Experience*, *22*(17), 2323–2334. https://doi.org/10.1002/cpe.1600

Albert, L. P., Wu, J., Prohaska, N., de Camargo, P. B., Huxman, T. E., Tribuzy, E. S., … Saleska, S. R. (2018). Age-dependent leaf physiology and consequences for crown-scale carbon uptake during the dry season in an Amazon evergreen forest. *New Phytologist*, *219*(3), 870–884. https://doi.org/10.1111/nph.15056

Ali, A. A., Xu, C., Rogers, A., Fisher, R. A., Wullschleger, S. D., Massoud, E. C., … Wilson, C. J. (2016). A global scale mechanistic model of photosynthetic capacity (LUNA V1.0). *Geoscientific Model Development*, *9*(2), 587–606. https://doi.org/10.5194/gmd-9-587-2016

Ali, A. A., Xu, C., Rogers, A., McDowell, N. G., Medlyn, B. E., Fisher, R. A., … Wilson, C. J. (2015). Global scale environmental control of plant photosynthetic capacity. *Ecological Applications*, *25*(8), 2349–2365. https://doi.org/10.1890/14-2111.1

Alton, P. B. (2017). Retrieval of seasonal Rubisco-limited photosynthetic capacity at global FLUXNET sites from hyperspectral satellite remote sensing: Impact on carbon modelling. *Agricultural and Forest Meteorology*, *232*, 74–88. https://doi.org/10.1016/j.agrformet.2016.08.001

Alton, P. B. (2018). Decadal trends in photosynthetic capacity and leaf area index inferred from satellite remote sensing for global vegetation types. *Agricultural and Forest Meteorology*, *250–251*(January), 361–375. https://doi.org/10.1016/j.agrformet.2017.11.020

Anav, A., Friedlingstein, P., Beer, C., Ciais, P., Harper, A., Jones, C., … Zhao, M. (2015). Spatio-temporal patterns of terrestrial gross primary production: A review. *Reviews of Geophysics*, *53*(3), 785–818. https://doi.org/10.1002/2015RG000483

Anderegg, W. R. L., Schwalm, C., Biondi, F., Camarero, J. J., Koch, G., Litvak, M., … Pacala, S. (2015). Pervasive drought legacies in forest ecosystems and their implications for carbon cycle models. *Science*, *349*(6247), 528–532. https://doi.org/10.1126/science.aab1833

Anten, N. P. R., Werger, M. J. A., & Medina, E. (1998). Nitrogen distribution and leaf area indices in relation to photosynthetic nitrogen use efficiency in savanna grasses. *Plant Ecology*, *138*(1), 63–75. https://doi.org/10.1023/A:1009727822617

Baldocchi, D., Ryu, Y., & Keenan, T. (2016). Terrestrial carbon cycle variability. *F1000Research*, *5*, 2371. https://doi.org/10.12688/f1000research.8962.1

Bernacchi, C. J., Morgan, P. B., Ort, D. R., & Long, S. P. (2005). The growth of soybean under free air [CO_2] enrichment (FACE)

stimulates photosynthesis while decreasing in vivo Rubisco capacity. *Planta*, *220*(3), 434–446. https://doi.org/10.1007/s00425-004-1320-8

Bernacchi, C. J., Pimentel, C., & Long, S. P. (2003). In vivo temperature response functions of parameters required to model RuBP-limited photosynthesis. *Plant, Cell and Environment*, *26*(9), 1419–1430. https://doi.org/10.1046/j.0016-8025.2003.01050.x

Bernacchi, C. J., Singsaas, E. L., Pimentel, C., Portis Jr., A. R., & Long, S. P. (2001). Improved temperature response functions for models of Rubisco-limited photosynthesis. *Plant, Cell and Environment*, *24*(2), 253–259. https://doi.org/10.1046/j.1365-3040.2001.00668.x

Bernotas, G., Scorza, L. C. T., Hansen, M. F., Hales, I. J., Halliday, K. J., Smith, L. N., … McCormick, A. J. (2019). A photometric stereo-based 3D imaging system using computer vision and deep learning for tracking plant growth. *GigaScience*, *8*(5), 1–15. https://doi.org/10.1093/gigascience/giz056

Bertheloot, J., Martre, P., & Andrieu, B. (2008). Dynamics of light and nitrogen distribution during grain filling within wheat canopy. *Plant Physiology*, *148*(3), 1707–1720. https://doi.org/10.1104/pp.108.124156

Bloomfield, K. J., Prentice, I. C., Cernusak, L. A., Eamus, D., Medlyn, B. E., Rumman, R., … Atkin, O. K. (2018). The validity of optimal leaf traits modelled on environmental conditions. *New Phytologist*, *221*(3), 1409–1423. https://doi.org/10.1111/nph.15495

Bonan, G. B., Lawrence, P. J., Oleson, K. W., Levis, S., Jung, M., Reichstein, M., … Swenson, S. C. (2011). Improving canopy processes in the Community Land Model version 4 (CLM4) using global flux fields empirically inferred from FLUXNET data. *Journal of Geophysical Research*, *116*(G2), G02014. https://doi.org/10.1029/2010JG001593

Bunting, E. L., Munson, S. M., & Villarreal, M. L. (2017). Climate legacy and lag effects on dryland plant communities in the southwestern U.S. *Ecological Indicators*, *74*, 216–229. https://doi.org/10.1016/j.ecolind.2016.10.024

Chen, J. L., Reynolds, J. F., Harley, P. C., & Tenhunen, J. D. (1993). Coordination theory of leaf nitrogen distribution in a canopy. *Oecologia*, *93*(1), 63–69. https://doi.org/10.1007/BF00321192

Coops, N. C., Jassal, R. S., Leuning, R., Black, A. T., & Morgenstern, K. (2007). Incorporation of a soil water modifier into MODIS predictions of temperate Douglas-fir gross primary productivity: Initial model development. *Agricultural and Forest Meteorology*, *147*(3–4), 99–109. https://doi.org/10.1016/j.agrformet.2007.07.001

Cornwell, W. (2017). A global dataset of leaf Δ13C values. *Zenodo*. https://doi.org/10.5281/zenodo.569501

Croft, H., Chen, J. M., Luo, X., Bartlett, P., Chen, B., & Staebler, R. M. (2017). Leaf chlorophyll content as a proxy for leaf photosynthetic capacity. *Global Change Biology*, *23*(9), 3513–3524. https://doi.org/10.1111/gcb.13599

De Pury, D. G. G., & Farquhar, G. D. (1997). Simple scaling of photosynthesis from leaves to canopies without the errors of big-leaf models. *Plant, Cell and Environment*, *20*(5), 537–557. https://doi.org/10.1111/j.1365-3040.1997.00094.x

Dechant, B., Cuntz, M., Vohland, M., Schulz, E., & Doktor, D. (2017). Estimation of photosynthesis traits from leaf reflectance spectra: Correlation to nitrogen content as the dominant mechanism. *Remote Sensing of Environment*, *196*, 279–292. https://doi.org/10.1016/j.rse.2017.05.019

Dillen, S. Y., de Beeck, M. O., Hufkens, K., Buonanduci, M., & Phillips, N. G. (2012). Seasonal patterns of foliar reflectance in relation to photosynthetic capacity and color index in two co-occurring tree species, *Quercus rubra* and *Betula papyrifera*. *Agricultural and Forest Meteorology*, *160*, 60–68. https://doi.org/10.1016/j.agrformet.2012.03.001

Dils, B., Buchwitz, M., Reuter, M., Schneising, O., Boesch, H., Parker, R., … Wunch, D. (2014). The greenhouse gas climate change initiative (GHG-CCI): Comparative validation of GHG-CCI SCIAMACHY/ENVISAT and TANSO-FTS/GOSAT CO_2 and CH_4 retrieval algorithm products with measurements from the TCCON. *Atmospheric Measurement Techniques*, *7*(6), 1723–1744. https://doi.org/10.5194/amt-7-1723-2014

Dong, N., Colin Prentice, I., Evans, B. J., Caddy-Retalic, S., Lowe, A. J., & Wright, I. J. (2017). Leaf nitrogen from first principles: Field evidence for adaptive variation with climate. *Biogeosciences*, *14*(2), 481–495. https://doi.org/10.5194/bg-14-481-2017

Dutta, D., Schimel, D. S., Sun, Y., Van Der Tol, C., & Frankenberg, C. (2019). Optimal inverse estimation of ecosystem parameters from observations of carbon and energy fluxes. *Biogeosciences*, *16*, 77–103. https://doi.org/10.5194/bg-16-77-2019

Evans, J. R. (1989). Photosynthesis and nitrogen relationship in leaves of C3 plants. *Oecologia*, *78*(1), 9–19. https://doi.org/10.1007/BF00377192

Evans, J. R., & Poorter, H. (2001). Photosynthetic acclimation of plants to growth irradiance: The relative importance of specific leaf area and nitrogen partitioning in maximizing carbon gain. *Plant, Cell and Environment*, *24*(8), 755–767. https://doi.org/10.1046/j.1365-3040.2001.00724.x

Farquhar, G. D., Caemmerer, S. V., & Berry, J. A. (1980). A biochemical model of photosynthetic CO_2 assimilation in leaves of C3 species. *Planta*, *90*, 78–90. https://doi.org/10.1007/BF00386231

Feret, J.-B., François, C., Asner, G. P., Gitelson, A. A., Martin, R. E., Bidel, L. P. R., … Jacquemoud, S. (2008). PROSPECT-4 and 5: Advances in the leaf optical properties model separating photosynthetic pigments. *Remote Sensing of Environment*, *112*(6), 3030–3043. https://doi.org/10.1016/j.rse.2008.02.012

Field, C. B. (1991). Ecological scaling of carbon gain to stress and resource availability. In *Response of plants to multiple stresses* (pp. 35–65). Academic Press. https://doi.org/10.1016/B978-0-08-092483-0.50007-4

Fisher, J. B., Huntzinger, D. N., Schwalm, C. R., & Sitch, S. (2014). Modeling the terrestrial biosphere. *Annual Review of Environment and Resources*, *39*(1), 91–123. https://doi.org/10.1146/annurev-environ-012913-093456

Flexas, J., Ribas-Carbó, M., Bota, J., Galmés, J., Henkle, M., Martínez-Cañellas, S., & Medrano, H. (2006). Decreased Rubisco activity during water stress is not induced by decreased relative water content but related to conditions of low stomatal conductance and chloroplast CO_2 concentration. *New Phytologist*, *172*(1), 73–82. https://doi.org/10.1111/j.1469-8137.2006.01794.x

Frankenberg, C., & Berry, J. (2018). *Solar induced chlorophyll fluorescence: Origins, relation to photosynthesis and retrieval. Comprehensive remote sensing*. Elsevier. https://doi.org/10.1016/B978-0-12-409548-9.10632-3

Fürstenau Togashi, H., Colin Prentice, I., Atkin, O. K., Macfarlane, C., Prober, S. M., Bloomfield, K. J., & Evans, B. J. (2018). Thermal acclimation of leaf photosynthetic traits in an evergreen woodland, consistent with the coordination hypothesis. *Biogeosciences*, *15*(11), 3461–3474. https://doi.org/10.5194/bg-15-3461-2018

Goetz, S. J., Prince, S. D., Goward, S. N., Thawley, M. M., & Small, J. (1999). Satellite remote sensing of primary production: An improved production efficiency modeling approach. *Ecological Modelling*, *122*, 239–255. https://doi.org/10.1016/S0304-3800(99)00140-4

Goudriaan, J. (1977). *Crop micrometeorology: A simulation study*. Retrieved from https://library.wur.nl/WebQuery/wurpubs/70980

Grassi, G., Vicinelli, E., Ponti, F., Cantoni, L., & Magnani, F. (2005). Seasonal and interannual variability of photosynthetic capacity in relation to leaf nitrogen in a deciduous forest plantation in northern Italy. *Tree Physiology*, *25*(3), 349–360. https://doi.org/10.1093/treephys/25.3.349

Gu, L., Han, J., Wood, J. D., Chang, C. Y. Y., & Sun, Y. (2019). Sun-induced Chl fluorescence and its importance for biophysical modeling of photosynthesis based on light reactions. *New Phytologist*, *223*(3), 1179–1191. https://doi.org/10.1111/nph.15796

Guo, J. S., & Ogle, K. (2019). Antecedent soil water content and vapor pressure deficit interactively control water potential in *Larrea tridentata*. *New Phytologist*, *221*(1), 218–232. https://doi.org/10.1111/nph.15374

Hansen, M. C., DeFries, R. S., Townshend, J. R. G., Carroll, M., Dimiceli, C., & Sohlberg, R. A. (2003). Global percent tree cover at a spatial resolution of 500 meters: First results of the MODIS vegetation continuous fields algorithm. *Earth Interactions*, *7*(10), 1–15. https://doi.org/10.1175/1087-3562(2003)007<0001:gptcaa>2.0.co;2

Harper, A. B., Cox, P. M., Friedlingstein, P., Wiltshire, A. J., Jones, C. D., Sitch, S., … Van Bodegom, P. (2016). Improved representation of plant functional types and physiology in the Joint UK Land Environment Simulator (JULES v4.2) using plant trait information. *Geoscientific Model Development*, *9*(7), 2415–2440. https://doi.org/10.5194/gmd-9-2415-2016

Haxeltine, A., & Prentice, I. C. (1996). A general model for the light-use efficiency of primary production. *Functional Ecology*, *10*(5), 551. https://doi.org/10.2307/2390165

He, L., Chen, J. M., Liu, J., Zheng, T., Wang, R., Joiner, J., … Rogers, C. (2019). Diverse photosynthetic capacity of global ecosystems mapped by satellite chlorophyll fluorescence measurements. *Remote Sensing of Environment*, *232*(July), 111344. https://doi.org/10.1016/j.rse.2019.111344

Hikosaka, K., Anten, N. P. R., Borjigidai, A., Kamiyama, C., Sakai, H., Hasegawa, T., … Ito, A. (2016). A meta-analysis of leaf nitrogen distribution within plant canopies. *Annals of Botany*, *118*(2), 239–247. https://doi.org/10.1093/aob/mcw099

Hilker, T., Coops, N. C., Wulder, M. A., Black, T. A., & Guy, R. D. (2008). The use of remote sensing in light use efficiency based models of gross primary production: A review of current status and future requirements. *Science of the Total Environment*, *404*(2–3), 411–423. https://doi.org/10.1016/j.scitotenv.2007.11.007

Houborg, R., McCabe, M., Cescatti, A., Gao, F., Schull, M., & Gitelson, A. (2015). Joint leaf chlorophyll content and leaf area index retrieval from Landsat data using a regularized model inversion system (REGFLEC). *Remote Sensing of Environment*, *159*, 203–221. https://doi.org/10.1016/j.rse.2014.12.008

Houborg, R., McCabe, M. F., Cescatti, A., & Gitelson, A. A. (2015). Leaf chlorophyll constraint on model simulated gross primary productivity in agricultural systems. *International Journal of Applied Earth Observation and Geoinformation*, *43*, 160–176. https://doi.org/10.1016/j.jag.2015.03.016

Huang, D., Knyazikhin, Y., Dickinson, R. E., Rautiainen, M., Stenberg, P., Disney, M., … Myneni, R. B. (2007). Canopy spectral invariants for remote sensing and model applications. *Remote Sensing of Environment*, *106*, 106–122. https://doi.org/10.1016/j.rse.2006.08.001

Hughes, T. P., Kerry, J. T., Connolly, S. R., Baird, A. H., Eakin, C. M., Heron, S. F., … Torda, G. (2019). Ecological memory modifies the cumulative impact of recurrent climate extremes. *Nature Climate Change*, *9*(1), 40–43. https://doi.org/10.1038/s41558-018-0351-2

Hwang, Y., Ryu, Y., Huang, Y., Kim, J., Iwata, H., & Kang, M. (2020). Comprehensive assessments of carbon dynamics in an intermittently-irrigated rice paddy. *Agricultural and Forest Meteorology*, *285–286*(October 2019), 107933. https://doi.org/10.1016/j.agrformet.2020.107933

Jacquemoud, S., & Baret, F. (1990). PROSPECT: A model of leaf optical properties spectra. *Remote Sensing of Environment*, *34*(2), 75–91. https://doi.org/10.1016/0034-4257(90)90100-Z

Jiang, C., & Ryu, Y. (2016). Multi-scale evaluation of global gross primary productivity and evapotranspiration products derived from Breathing Earth System Simulator (BESS). *Remote Sensing of Environment*, *186*, 528–547. https://doi.org/10.1016/j.rse.2016.08.030

Joiner, J., Yoshida, Y., Guanter, L., & Middleton, E. M. (2016). New methods for the retrieval of chlorophyll red fluorescence from hyperspectral satellite instruments: Simulations and application to GOME-2 and SCIAMACHY. *Atmospheric Measurement Techniques*, *9*(8), 3939–3967. https://doi.org/10.5194/amt-9-3939-2016

Jongschaap, R. E. E., & Booij, R. (2004). Spectral measurements at different spatial scales in potato: Relating leaf, plant and canopy nitrogen status. *International Journal of Applied Earth Observation and Geoinformation*, *5*(3), 205–218. https://doi.org/10.1016/j.jag.2004.03.002

Katahata, S. I., Naramoto, M., Kakubari, Y., & Mukai, Y. (2007). Seasonal changes in photosynthesis and nitrogen allocation in leaves of different ages in evergreen understory shrub *Daphniphyllum humile*. *Trees – Structure and Function*, *21*(6), 619–629. https://doi.org/10.1007/s00468-007-0155-x

Kattge, J., Díaz, S., Lavorel, S., Prentice, I. C., Leadley, P., Bönisch, G., … Wirth, C. (2011). TRY – A global database of plant traits. *Global Change Biology*, *17*(9), 2905–2935. https://doi.org/10.1111/j.1365-2486.2011.02451.x

Kattge, J., & Knorr, W. (2007). Temperature acclimation in a biochemical model of photosynthesis: A reanalysis of data from 36 species. *Plant, Cell & Environment*, *30*(9), 1176–1190. https://doi.org/10.1111/j.1365-3040.2007.01690.x

Kattge, J., Knorr, W., Raddatz, T., & Wirth, C. (2009). Quantifying photosynthetic capacity and its relationship to leaf nitrogen content for global-scale terrestrial biosphere models. *Global Change Biology*, *15*(4), 976–991. https://doi.org/10.1111/j.1365-2486.2008.01744.x

Keenan, T. F., Prentice, I. C., Canadell, J. G., Williams, C. A., Wang, H., Raupach, M., & Collatz, G. J. (2016). Recent pause in the growth rate of atmospheric CO_2 due to enhanced terrestrial carbon uptake. *Nature Communications*, *7*, 13428. https://doi.org/10.1038/ncomms13428

Keenan, T., Sabate, S., & Gracia, C. (2010). Soil water stress and coupled photosynthesis-conductance models: Bridging the gap between conflicting reports on the relative roles of stomatal, mesophyll conductance and biochemical limitations to photosynthesis. *Agricultural and Forest Meteorology*, *150*(3), 443–453. https://doi.org/10.1016/j.agrformet.2010.01.008

Kim, J. (2007). KoFlux 2006 synthesis: HydroKorea and CarboKorea foreword. *Korean Journal of Agricultural and Forest Meteorology*, *9*(2), 71–74. https://doi.org/10.5532/kjafm.2007.9.2.071

Kitao, M., Kitaoka, S., Harayama, H., Tobita, H., Agathokleous, E., & Utsugi, H. (2018). Canopy nitrogen distribution is optimized to prevent photoinhibition throughout the canopy during sun flecks. *Scientific Reports*, *8*(1). https://doi.org/10.1038/s41598-017-18766-0

Kolari, P., Chan, T., Porcar-Castell, A., Bäck, J., Nikinmaa, E., & Juurola, E. (2014). Field and controlled environment measurements show strong seasonal acclimation in photosynthesis and respiration potential in boreal Scots pine. *Frontiers in Plant Science*, *5*(December), 1–12. https://doi.org/10.3389/fpls.2014.00717

Kosugi, Y., Shibata, S., & Kobashi, S. (2003). Parameterization of the CO_2 and H_2O gas exchange of several temperate deciduous broad-leaved trees at the leaf scale considering seasonal changes. *Plant, Cell and Environment*, *26*(2), 285–301. https://doi.org/10.1046/j.1365-3040.2003.00960.x

Kropp, H., Loranty, M., Alexander, H. D., Berner, L. T., Natali, S. M., & Spawn, S. A. (2017). Environmental constraints on transpiration and stomatal conductance in a Siberian Arctic boreal forest. *Journal of Geophysical Research: Biogeosciences*, *122*(3), 487–497. https://doi.org/10.1002/2016JG003709

Lavergne, A., Voelker, S., Csank, A., Graven, H., Boer, H. J., Daux, V., … Prentice, I. C. (2020). Historical changes in the stomatal limitation of photosynthesis: Empirical support for an optimality principle. *New Phytologist*, *225*(6), 2484–2497. https://doi.org/10.1111/nph.16314

Lavergne, S., Mouquet, N., Thuiller, W., & Ronce, O. (2010). Biodiversity and climate change: Integrating evolutionary and ecological responses

of species and communities. *Annual Review of Ecology, Evolution, and Systematics*, *41*(1), 321–350. https://doi.org/10.1146/annurev-ecolsys-102209-144628

Lemaire, G., Onillon, B., Gosse, G., Chartier, M., & Allirand, J. M. (1991). Nitrogen distribution within a lucerne canopy during regrowth: relation with light distribution. *Annals of Botany*, *68*(6), 483–488. https://doi.org/10.1093/oxfordjournals.aob.a088286

Leuning, R., Cleugh, H. A., Zegelin, S. J., & Hughes, D. (2005). Carbon and water fluxes over a temperate Eucalyptus forest and a tropical wet/dry savanna in Australia: Measurements and comparison with MODIS remote sensing estimates. *Agricultural and Forest Meteorology*, *129*(3–4), 151–173. https://doi.org/10.1016/j.agrformet.2004.12.004

Lin, Y. S., Medlyn, B. E., De Kauwe, M. G., & Ellsworth, D. S. (2013). Biochemical photosynthetic responses to temperature: How do interspecific differences compare with seasonal shifts? *Tree Physiology*, *33*(8), 793–806. https://doi.org/10.1093/treephys/tpt047

Liu, Y., Schwalm, C. R., Samuels-Crow, K. E., & Ogle, K. (2019). Ecological memory of daily carbon exchange across the globe and its importance in drylands. *Ecology Letters*, *22*(11), 1806–1816. https://doi.org/10.1111/ele.13363

Lloyd, J., Patiño, S., Paiva, R. Q., Nardoto, G. B., Quesada, C. A., Santos, A. J. B., … Mercado, L. M. (2010). Optimisation of photosynthetic carbon gain and within-canopy gradients of associated foliar traits for Amazon forest trees. *Biogeosciences*, *7*(6), 1833–1859. https://doi.org/10.5194/bg-7-1833-2010

Luo, X., Croft, H., Chen, J. M., Bartlett, P., Staebler, R., & Froelich, N. (2018). Incorporating leaf chlorophyll content into a two-leaf terrestrial biosphere model for estimating carbon and water fluxes at a forest site. *Agricultural and Forest Meteorology*, *248*(May 2017), 156–168. https://doi.org/10.1016/j.agrformet.2017.09.012

Luo, X., Croft, H., Chen, J. M., He, L., & Keenan, T. F. (2019). Improved estimates of global terrestrial photosynthesis using information on leaf chlorophyll content. *Global Change Biology*, *25*(3), 1–16. https://doi.org/10.1111/gcb.14624

Maire, V., Martre, P., Kattge, J., Gastal, F., Esser, G., Fontaine, S., & Soussana, J. F. (2012). The coordination of leaf photosynthesis links C and N fluxes in C3 plant species. *PLoS One*, *7*(6), 1–15. https://doi.org/10.1371/journal.pone.0038345

Medlyn, B. E. (1998). Physiological basis of the light use efficiency model. *Tree Physiology*, *18*(3), 167–176. https://doi.org/10.1093/treephys/18.3.167

Medlyn, B. E., Dreyer, E., Ellsworth, D., Forstreuter, M., Harley, P. C., Kirschbaum, M. U. F., … Loustau, D. (2002). Temperature response of parameters of a biochemically based model of photosynthesis. II. A review of experimental data. *Plant, Cell and Environment*, *25*(9), 1167–1179. https://doi.org/10.1046/j.1365-3040.2002.00891.x

Monteith, J. L. (1972). Solar radiation and productivity in tropical ecosystems. *The Journal of Applied Ecology*, *9*(3), 747. https://doi.org/10.2307/2401901

Monteith, J. L. (1977). Climate and the efficiency of crop production in Britain. *Philosophical Transactions of the Royal Society of London. B*, *281*(980), 277–294.

Muraoka, H., Saigusa, N., Nasahara, K. N., Noda, H., Yoshino, J., Saitoh, T. M., … Koizumi, H. (2010). Effects of seasonal and interannual variations in leaf photosynthesis and canopy leaf area index on gross primary production of a cool-temperate deciduous broadleaf forest in Takayama, Japan. *Journal of Plant Research*, *123*(4), 563–576. https://doi.org/10.1007/s10265-009-0270-4

Myneni, R. B., Hoffman, S., Knyazikhin, Y., Privette, J. L., Glassy, J., Tian, Y., … Running, S. W. (2002). Global products of vegetation leaf area and fraction absorbed PAR from year one of MODIS data. *Remote Sensing of Environment*, *83*, 214–231. https://doi.org/10.1016/S0034-4257(02)00074-3

Ogle, K., & Barber, J. J. (2016). Plant and ecosystem memory. *CHANCE*, *29*(2), 16–22. https://doi.org/10.1080/09332480.2016.1181961

Ogle, K., Barber, J. J., Barron-Gafford, G. A., Bentley, L. P., Young, J. M., Huxman, T. E., … Tissue, D. T. (2015). Quantifying ecological memory in plant and ecosystem processes. *Ecology Letters*, *18*(3), 221–235. https://doi.org/10.1111/ele.12399

Pastorello, G., Papale, D., Chu, H., Trotta, C., Agarwal, D., Canfora, E., … Torn, M. (2017). A new data set to keep a sharper eye on land-air exchanges. *Eos, Transactions American Geophysical Union (Online)*, *98*(8). https://doi.org/10.1029/2017EO071597

Pavlick, R., Drewry, D. T., Bohn, K., Reu, B., & Kleidon, A. (2013). The Jena Diversity-Dynamic Global Vegetation Model (JeDi-DGVM): A diverse approach to representing terrestrial biogeography and biogeochemistry based on plant functional trade-offs. *Biogeosciences*, *10*(6), 4137–4177. https://doi.org/10.5194/bg-10-4137-2013

Prentice, I. C., Dong, N., Gleason, S. M., Maire, V., & Wright, I. J. (2014). Balancing the costs of carbon gain and water transport: Testing a new theoretical framework for plant functional ecology. *Ecology Letters*, *17*(1), 82–91. https://doi.org/10.1111/ele.12211

Rogers, A., Medlyn, B. E., Dukes, J. S., Bonan, G. B., von Caemmerer, S., Dietze, M. C., … Zaehle, S. (2016). A roadmap for improving representation of photosynthesis in Earth system models. *New Phytologist*, *213*, 22–42. https://doi.org/10.1111/nph.14283

Running, S. W., Nemani, R. R., Heinsch, F. A., Zhao, M., Reeves, M., & Hashimoto, H. (2004). A continuous satellite-derived measure of global terrestrial primary production. *BioScience*, *54*(6), 547. https://doi.org/10.1641/0006-3568(2004)054[0547:ACSMOG]2.0.CO;2

Ryan, E. M., Ogle, K., Zelikova, T. J., Lecain, D. R., Williams, D. G., Morgan, J. A., & Pendall, E. (2015). Antecedent moisture and temperature conditions modulate the response of ecosystem respiration to elevated CO_2 and warming. *Global Change Biology*, *21*(7), 2588–2602. https://doi.org/10.1111/gcb.12910

Ryu, Y., Berry, J. A., & Baldocchi, D. D. (2019). What is global photosynthesis? History, uncertainties and opportunities. *Remote Sensing of Environment*, *223*(November 2018), 95–114. https://doi.org/10.1016/j.rse.2019.01.016

Ryu, Y., Jiang, C., Kobayashi, H., & Detto, M. (2018). MODIS-derived global land products of shortwave radiation and diffuse and total photosynthetically active radiation at 5 km resolution from 2000. *Remote Sensing of Environment*, *204*(January 2018), 812–825. https://doi.org/10.1016/j.rse.2017.09.021

Ryu, Y., Lee, G., Jeon, S., Song, Y., & Kimm, H. (2014). Monitoring multi-layer canopy spring phenology of temperate deciduous and evergreen forests using low-cost spectral sensors. *Remote Sensing of Environment*, *149*, 227–238. https://doi.org/10.1016/j.rse.2014.04.015

Ryu, Y., Nilson, T., Kobayashi, H., Sonnentag, O., Law, B. E., & Baldocchi, D. D. (2010). On the correct estimation of effective leaf area index: Does it reveal information on clumping effects? *Agricultural and Forest Meteorology*, *150*(3), 463–472. https://doi.org/10.1016/j.agrformet.2010.01.009

Schaaf, C. B., Gao, F., Strahler, A. H., Lucht, W., Li, X., Tsang, T., … Roy, D. (2002). First operational BRDF, albedo nadir reflectance products from MODIS. *Remote Sensing of Environment*, *83*(1–2), 135–148. https://doi.org/10.1016/S0034-4257(02)00091-3

Scheiter, S., Langan, L., & Higgins, S. I. (2013). Next-generation dynamic global vegetation models: Learning from community ecology. *New Phytologist*, *198*(3), 957–969. https://doi.org/10.1111/nph.12210

Serbin, S. P., Singh, A., Desai, A. R., Dubois, S. G., Jablonski, A. D., Kingdon, C. C., … Townsend, P. A. (2015). Remotely estimating photosynthetic capacity, and its response to temperature, in vegetation canopies using imaging spectroscopy. *Remote Sensing of Environment*, *167*, 78–87. https://doi.org/10.1016/j.rse.2015.05.024

Singsaas, E. L., Ort, D. R., & DeLucia, E. H. (2001). Variation in measured values of photosynthetic quantum yield in ecophysiological studies. *Oecologia*, *128*(1), 15–23. https://doi.org/10.1007/s004420000624

Smith, N. G., Keenan, T. F., Colin Prentice, I., Wang, H., Wright, I. J., Niinemets, Ü., … Zhou, S.-X. (2019). Global photosynthetic capacity is optimized to the environment. *Ecology Letters*, *22*(3), 506–517. https://doi.org/10.1111/ele.13210

Smolander, S., & Stenberg, P. (2005). Simple parameterizations of the radiation budget of uniform broadleaved and coniferous canopies. *Remote Sensing of Environment*, *94*, 355–363. https://doi.org/10.1016/j.rse.2004.10.010

Stocker, B. D., Wang, H., Smith, N. G., Harrison, S. P., Keenan, T. F., Sandoval, D., … Prentice, I. C. (2019). P-model v1. 0: An optimality-based light use efficiency model for simulating ecosystem gross primary production. *Geoscientific Model Development Discussions*, 1–59. https://doi.org/10.5194/gmd-2019-200

Stocker, B. D., Zscheischler, J., Keenan, T. F., Prentice, I. C., Seneviratne, S. I., & Peñuelas, J. (2019). Drought impacts on terrestrial primary production underestimated by satellite monitoring. *Nature Geoscience*, *12*(4), 264–270. https://doi.org/10.1038/s41561-019-0318-6

Sulkava, M., Luyssaert, S., Zaehle, S., & Papale, D. (2011). Assessing and improving the representativeness of monitoring networks: The European flux tower network example. *Journal of Geophysical Research*, *116*(2), G00J04. https://doi.org/10.1029/2010JG001562

Van Bodegom, P. M., Douma, J. C., & Verheijen, L. M. (2014). A fully traits-based approach to modeling global vegetation distribution. *Proceedings of the National Academy of Sciences of the United States of America*, *111*(38), 13733–13738. https://doi.org/10.1073/pnas.1304551110

van der Tol, C., Rossini, M., Cogliati, S., Verhoef, W., Colombo, R., Rascher, U., & Mohammed, G. (2016). A model and measurement comparison of diurnal cycles of sun-induced chlorophyll fluorescence of crops. *Remote Sensing of Environment*, *186*, 663–677. https://doi.org/10.1016/j.rse.2016.09.021

Verheijen, L. M., Brovkin, V., Aerts, R., Bönisch, G., Cornelissen, J. H. C., Kattge, J., … van Bodegom, P. M. (2013). Impacts of trait variation through observed trait-climate relationships on performance of an Earth system model: A conceptual analysis. *Biogeosciences*, *10*(8), 5497–5515. https://doi.org/10.5194/bg-10-5497-2013

von Caemmerer, S., Farquhar, G., & Berry, J. (2009). Biochemical model of C3 photosynthesis. In *Photosynthesis in silico: Understanding complexity from molecules to ecosystems* (pp. 209–230). Dordrecht, The Netherlands: Springer. https://doi.org/10.1007/978-1-4020-9237-4_9

Walker, A. P., Hanson, P. J., De Kauwe, M. G., Medlyn, B. E., Zaehle, S., Asao, S., … Norby, R. J. (2014). Comprehensive ecosystem model-data synthesis using multiple data sets at two temperate forest free-air CO_2 enrichment experiments: Model performance at ambient CO_2 concentration. *Journal of Geophysical Research: Biogeosciences*, *119*(5), 937–964. https://doi.org/10.1002/2013JG002553

Walker, A. P., Quaife, T., van Bodegom, P. M., De Kauwe, M. G., Keenan, T. F., Joiner, J., … Woodward, F. I. (2017). The impact of alternative trait-scaling hypotheses for the maximum photosynthetic carboxylation rate (V_{cmax}) on global gross primary production. *New Phytologist*, *215*(4), 1370–1386. https://doi.org/10.1111/nph.14623

Walker, B. J., Drewry, D. T., Slattery, R. A., VanLoocke, A., Cho, Y. B., & Ort, D. R. (2018). Chlorophyll can be reduced in crop canopies with little penalty to photosynthesis. *Plant Physiology*, *176*(2), 1215–1232. https://doi.org/10.1104/pp.17.01401

Wang, H., Atkin, O. K., Keenan, T. F., Smith, N. G., Wright, I. J., Bloomfield, K. J., … Prentice, I. C. (2020). Acclimation of leaf respiration consistent with optimal photosynthetic capacity. *Global Change Biology*, *26*(4), 2573–2583. https://doi.org/10.1111/gcb.14980

Wang, H., Prentice, I. C., Davis, T. W., Keenan, T. F., Wright, I. J., & Peng, C. (2017). Photosynthetic responses to altitude: An explanation based on optimality principles. *New Phytologist*, *213*(3), 976–982. https://doi.org/10.1111/nph.14332

Wang, H., Prentice, I. C., Keenan, T. F., Davis, T. W., Wright, I. J., Cornwell, W. K., … Peng, C. (2017). Towards a universal model for carbon dioxide uptake by plants. *Nature Plants*, *3*(9), 734–741. https://doi.org/10.1038/s41477-017-0006-8

Wei, S., Fang, H., Schaaf, C. B., He, L., & Chen, J. M. (2019). Global 500 m clumping index product derived from MODIS BRDF data (2001–2017). *Remote Sensing of Environment*, *232*(December 2018), 2001–2017. https://doi.org/10.1016/j.rse.2019.111296

Wilson, K. B., Baldocchi, D. D., & Hanson, P. J. (2000). Spatial and seasonal variability of photosynthetic parameters and their relationship to leaf nitrogen in a deciduous forest. *Tree Physiology*, *20*(9), 565–578. https://doi.org/10.1093/treephys/20.9.565

Wilson, K. B., Baldocchi, D. D., & Hanson, P. J. (2001). Leaf age affects the seasonal pattern of photosynthetic capacity and net ecosystem exchange of carbon in a deciduous forest. *Plant, Cell and Environment*, *24*(6), 571–583. https://doi.org/10.1046/j.0016-8025.2001.00706.x

Wright, I. J., Reich, P. B., Cornelissen, J. H. C., Falster, D. S., Garnier, E., Hikosaka, K., … Westoby, M. (2005). Assessing the generality of global leaf trait relationships. *New Phytologist*, *166*(2), 485–496. https://doi.org/10.1111/j.1469-8137.2005.01349.x

Wu, D., Zhao, X., Liang, S., Zhou, T., Huang, K., Tang, B., & Zhao, W. (2015). Time-lag effects of global vegetation responses to climate change. *Global Change Biology*, *21*(9), 3520–3531. https://doi.org/10.1111/gcb.12945

Wu, J., Albert, L. P., Lopes, A. P., Restrepo-Coupe, N., Hayek, M., Wiedemann, K. T., … Saleska, S. R. (2016). Leaf development and demography explain photosynthetic seasonality in Amazon evergreen forests. *Science*, *351*(6276), 972–976. https://doi.org/10.1126/science.aad5068

Wullschleger, S. D., Epstein, H. E., Box, E. O., Euskirchen, E. S., Goswami, S., Iversen, C. M., … Xu, X. (2014). Plant functional types in Earth system models: Past experiences and future directions for application of dynamic vegetation models in high-latitude ecosystems. *Annals of Botany*, *114*(1), 1–16. https://doi.org/10.1093/aob/mcu077

Xiao, J., Chevallier, F., Gomez, C., Guanter, L., Hicke, J. A., Huete, A. R., … Zhang, X. (2019). Remote sensing of the terrestrial carbon cycle: A review of advances over 50 years. *Remote Sensing of Environment*, *233*(September), 111383. https://doi.org/10.1016/j.rse.2019.111383

Xu, L., & Baldocchi, D. D. (2003). Seasonal trends in photosynthetic parameters and stomatal conductance of blue oak (*Quercus douglasii*) under prolonged summer drought and high temperature. *Tree Physiology*, *23*(13), 865–877. https://doi.org/10.1093/treephys/23.13.865

Yang, K., Ryu, Y., Dechant, B., Berry, J. A., Hwang, Y., Jiang, C., … Yang, X. I. (2018). Sun-induced chlorophyll fluorescence is more strongly related to absorbed light than to photosynthesis at half-hourly resolution in a rice paddy. *Remote Sensing of Environment*, *216*(June), 658–673. https://doi.org/10.1016/j.rse.2018.07.008

Yang, W., Yang, L., & Merchant, J. W. (1997). An assessment of AVHRR/NDVI-ecoclimatological relations in Nebraska, U.S.A. *International Journal of Remote Sensing*, *18*(10), 2161–2180. https://doi.org/10.1080/014311697217819

Yang, Y., Zhu, Q., Peng, C., Wang, H., & Chen, H. (2015). From plant functional types to plant functional traits: A new paradigm in modelling global vegetation dynamics. *Progress in Physical Geography*, *39*(4), 514–535. https://doi.org/10.1177/0309133315582018

Zeng, Y., Badgley, G., Dechant, B., Ryu, Y., Chen, M., & Berry, J. A. (2019). A practical approach for estimating the escape ratio of near-infrared solar-induced chlorophyll fluorescence. *Remote Sensing of Environment*, *232*(July 2018), 111209. https://doi.org/10.1016/j.rse.2019.05.028

Zhang, L., Hu, Z., Fan, J., Zhou, D., & Tang, F. (2014). A meta-analysis of the canopy light extinction coefficient in terrestrial ecosystems. *Frontiers of Earth Science*, *8*(4), 599–609. https://doi.org/10.1007/s11707-014-0446-7

Zhang, Y., Guanter, L., Berry, J. A., Joiner, J., van der Tol, C., Huete, A., … Köhler, P. (2014). Estimation of vegetation photosynthetic capacity

from space-based measurements of chlorophyll fluorescence for terrestrial biosphere models. *Global Change Biology*, *20*(12), 3727–3742. https://doi.org/10.1111/gcb.12664

Zhang, Y., Guanter, L., Joiner, J., Song, L., & Guan, K. (2018). Spatially-explicit monitoring of crop photosynthetic capacity through the use of space-based chlorophyll fluorescence data. *Remote Sensing of Environment*, *210*(June 2017), 362–374. https://doi.org/10.1016/j.rse.2018.03.031

Zhang, Y., Joiner, J., Gentine, P., & Zhou, S. (2018). Reduced solar-induced chlorophyll fluorescence from GOME-2 during Amazon drought caused by dataset artifacts. *Global Change Biology*, *24*(6), 2229–2230. https://doi.org/10.1111/gcb.14134

Zhang, Y., Song, C., Sun, G., Band, L. E., Noormets, A., & Zhang, Q. (2015). Understanding moisture stress on light-use efficiency across terrestrial ecosystems based on global flux and remote sensing data. *Journal of Geophysical Research: Biogeosciences*, *120*(10), 2053–2066. https://doi.org/10.1002/2015JG003023

Zheng, T., Chen, J., He, L., Arain, M. A., Thomas, S. C., Murphy, J. G., … Black, T. A. (2017). Inverting the maximum carboxylation rate (V_{cmax}) from the sunlit leaf photosynthesis rate derived from measured light response curves at tower flux sites. *Agricultural and Forest Meteorology*, *236*, 48–66. https://doi.org/10.1016/j.agrformet.2017.01.008

Zhou, Y., Ju, W., Sun, X., Hu, Z., Han, S., Andrew Black, T., … Wu, X. (2014). Close relationship between spectral vegetation indices and V_{cmax} in deciduous and mixed forests. *Tellus, Series B: Chemical and Physical Meteorology*, *66*(1), 1–16. https://doi.org/10.3402/tellusb.v66.23279

SUPPORTING INFORMATION

Additional supporting information may be found online in the Supporting Information section.

How to cite this article: Jiang C, Ryu Y, Wang H, Keenan TF. An optimality-based model explains seasonal variation in C3 plant photosynthetic capacity. *Glob Change Biol*. 2020;26: 6493–6510. https://doi.org/10.1111/gcb.15276